1 **Antarctic ice rises and rumples: their properties and significance for**
2 **ice-sheet dynamics and evolution**

3 Kenichi Matsuoka[a], Richard C.A. Hindmarsh[b], Geir Moholdt[a], Michael J. Bentley[c], Hamish D.
4 Pritchard[b], Joel Brown[a*], Howard Conway[d], Reinhard Drews[e], Gaël Durand[f, g], Daniel Goldberg[h],
5 Tore Hattermann[i,j], Jonathan Kingslake[b], Jan T.M. Lenaerts[k], Carlos Martín[b], Robert Mulvaney[b],
6 Keith Nicholls[b], Frank Pattyn[e], Neil Ross[l], Ted Scambos[m], Pippa L. Whitehouse[c]

7 a. Norwegian Polar Institute, Framsenteret, Tromsø, 9296, NORWAY
8 b. British Antarctic Survey, High Cross, Madingley Road, Cambridge, CB3 0ET, UK
9 c. Department of Geography, Durham University, Lower Mountjoy, South Road, Durham,
10 DH1 3LE, UK
11 d. Department of Earth and Space Sciences, University of Washington, Seattle, WA, 98195-
12 1310, USA
13 e. Laboratoire de Glaciologie, Université Libre de Bruxelles, Avenue F.D. Roosevelt 50, B-
14 1050 Brussels, BELGIUM
15 f. CNRS, LGGE, F-38041, Grenoble, FRANCE
16 g. University Grenoble Alps, LGGE, F-38041, Grenoble, FRANCE
17 h. School of Geoscience, University of Edinburgh, Drummond Street, Edinburgh, EH8 9XP,
18 UK
19 i. Akvaplan-Niva AS, Framsenteret, Tromsø, 9296, NORWAY
20 j. Alfred Wegener Institute for Polar and Marine Research, Bremerhaven, GERMANY.
21 k. Institute for Marine and Atmospheric Research, Utrecht University, P.O. Box 80005,
22 3508 TA Utrecht, THE NETHERLANDS
23 l. School of Geography, Politics, and Sociology, Newcastle University, Newcastle Upon
24 Tyne, NE1 7RU, UK.
25 m. National Snow and Ice Data Center, Cooperative Institute for Research in Environmental
26 Sciences, University of Colorado, Boulder, CO 80309-0449, USA

27 * Current affiliation: Aesir Consulting LLC, Missoula, MT, USA.

## Key words
29 Antarctic Ice Sheet; Holocene deglaciation; sea-level rise, pinning point, ice dome

## Abstract
31 Locally grounded features in ice shelves, called ice rises and rumples, play a key role buttressing
32 discharge from the Antarctic Ice Sheet and regulating its contribution to sea level. Ice rises
33 typically rise several hundreds of meters above the surrounding ice shelf; shelf flow is diverted
34 around them. On the other hand, shelf ice flows across ice rumples, which typically rise only a
35 few tens of meters above the ice shelf. Ice rises contain rich histories of deglaciation and climate
36 that extend back over timescales ranging from a few millennia to beyond the last glacial
37 maximum. Numerical model results have shown that the buttressing effects of ice rises and
38 rumples are significant, but details of processes and how they evolve remain poorly understood.
39 Fundamental information about the conditions and processes that cause transitions between
40 floating ice shelves, ice rises and ice rumples is needed in order to assess their impact on ice-
41 sheet behavior. Targeted high-resolution observational data are needed to evaluate and improve
42 prognostic numerical models and parameterizations of the effects of small-scale pinning points
43 on grounding-zone dynamics.

## 1.    Introduction

Small-scale topographic features occur wherever ice shelves ground locally on the elevated seabed. These features are called "ice rises" where the flowing ice shelf is diverted around the grounded region, and "ice rumples" where the ice shelf flows over the grounded region (Figs. 1 and 2). Numerous ice rises around the edge of the Antarctic Ice Sheet are in fact miniature ice sheets — independent entities with many of the characteristics shared with the larger, main ice sheet (Robin, 1953). Being smaller and numerous, ice rises represent a far larger sample of possible ice sheets. Each one is relatively simple, but the population provides much variety. As such, they provide a convenient platform for conducting geophysical and glaciological observations and model experiments to develop concepts about ice sheets.

Understanding the role of ice rises in the evolution and future of the Antarctic Ice Sheet is important for three primary reasons. First, glacial-interglacial changes in the extent and configuration of the Antarctic Ice Sheet are largest at the margins, so knowledge from ice rises provide powerful constraints on the timing and amount of thickness changes (e.g., Conway et al., 1999; Brook et al., 2005; Waddington et al., 2005; Martin et al., 2006; Mulvaney et al., 2007). Second, relatively high surface mass balance (SMB) and close proximity to the storm track that circulates Antarctica make ice cores from ice rises well suited to examine highly regional, circumpolar variations in Antarctic climate and sea ice, and their tele-connections (e.g., Goodwin et al., 2014; Sinclair et al., 2014). Finally, the mass balance of Antarctica is dominated by grounding-zone dynamics and ice-shelf/ocean interactions, which are influenced by ice rises and rumples. For example it is thought that recent un-grounding of an ice rumple within the ice shelf of Pine Island Glacier in the Amundsen Sea Embayment has contributed to the ongoing retreat and thinning in the region (Jenkins et al., 2010a; Gladstone et al., 2012). Losses from the Amundsen Sea Embayment dominate the current mass deficit of the Antarctic Ice Sheet (Pritchard et al., 2012; Joughin et al., 2014; Rignot et al., 2014; Fürst et al., 2015). Ice rumples are much smaller than ice rises, but provide significant buttressing to the ice shelf with potential for rapid ice-dynamical changes in cases of grounding or un-grounding.

Here, we review current understanding of ice rises and rumples in terms of their morphology, distribution, history, and impact on the evolution of Antarctica. Section 2 first defines ice rises and rumples and then shows their distributions, and their geological, oceanographic, and climatological settings. We also discuss their formation mechanisms. Section 3 reviews the roles of ice rises and rumples in ice-sheet dynamics and mass balance. Section 4 provides an overview of current knowledge of the Holocene retreat of the Antarctic Ice Sheet, with emphasis on the records and roles of ice rises. Finally, in Section 5, we discuss major knowledge gaps and key directions and needs for future research.

## 2.    Settings

### 2.1    Definition of ice rises and rumples

Ice rises and ice rumples are locally elevated, grounded features surrounded fully or partially by ice shelves or ice streams (Figs. 1 and 2). Other terms such as ice hill, ice dome, ice promontory, ice ridge, and inter-ice-stream ridge have also been used to refer to ice rises (depending on which characteristic is being emphasized), so we include them in our definition here. We follow MacAyeal (1987) to distinguish ice rises and rumples.

Ice rises are built mostly from locally accumulating snow. They consist of radial ice-flow centers or divides separate from the main ice sheet. They are typically several hundred meters

88  higher than the surrounding ice shelves or ice streams. In cross section (Fig. 2), the surface
89  topography is quasi parabolic with flank slopes extending from a blunt peak (Martin and
90  Sanderson, 1980). Local snow accumulation and negligible horizontal ice flow make the flow
91  divide or center an excellent site to extract ice cores to determine coastal Antarctic climate.
92  Examples of ice rises of various types include (see Figures 1 and 3 for locations): (#1) Roosevelt
93  Island in the Ross Sea Embayment and Korff Ice Rise in the Weddell Sea Embayment are isles
94  completely surrounded by ice shelves; (#2) Fletcher Promontory in the Weddell Sea Embayment
95  is a promontory of the ice sheet protruding into the ice shelf; (#3) Siple Dome in the Ross Sea
96  Embayment is an inter-ice-stream ridge; and (#4) Dorsey Island in the Wilkins Ice Shelf is an
97  island that consists of both ice and outcrops of bedrock or sediments. Ice rises in categories #2
98  and #3 are elongate extensions of the inland ice sheet into the ice shelf, but have saddles between
99  the adjacent inland ice sheet and seaward local flow centers at elevations that are higher than the
100 proximal grounded ice sheet.

101        Ice rumples, on the other hand, are fully enclosed within ice shelves and are typically
102 elevated only tens of meters or less from the ice-shelf surface. Some ice rumples exist at the
103 calving front of the ice shelf, partly facing the ocean. Others are located near ice rises or within
104 grounding zones or lightly grounded ice plains (Brunt et al., 2011). Ice flows across rumples and
105 maintains the same general flow direction as that in the adjacent ice shelf (Fig. 1b). Shearing can
106 occur at the base and most of the ice within rumples is not locally accumulated. Examples are
107 Doake Ice Rumples between Korff and Henry Ice Rises in the central part of the Ronne-Filchner
108 Ice Shelf (Fig. 1). Field observations across ice rumples are sparse (Limbert, 1964; Thomas,
109 1973b; Swithinbank, 1977; Smith, 1986; Smith, 1991), mainly because the presence of crevasses
110 and rifts hamper surface travel. A notable exception is an ice rumple that was present near the
111 grounding zone of Pine Island Glacier; ice shelf and seabed topography were mapped by an
112 airborne survey and autonomous underwater vehicle (Jenkins et al., 2010a; Jacobs et al., 2011).
113 Here, we do not consider features that ground ephemerally over tidal cycles as ice rumples,
114 because such features provide little buttressing to the ice shelf (Section 3) and their detection
115 using satellite techniques depends on the timing of the observation. Nevertheless, these
116 ephemerally grounded features can readily become ice rumples if the ice shelf thickens or relative
117 sea level lowers.

## 2.2    Identification by satellite remote sensing

119 The elevated topography of ice rises and rumples and their ice-flow perturbations in ice shelves
120 such as crevasses and rifts are well imaged by a variety of satellites (Fig. 1a). Visible, near-
121 infrared-band, and microwave imagery, such as that from AVHRR, MODIS, Landsat, ASTER,
122 SPOT, and Radarsat all show brightness changes associated with surface-slope variations in the
123 grounding zone, and also at the crest of ice rises (e.g., Martin, 1976; Scambos et al., 2007). In
124 addition, abrupt elevation variations relative to ice shelves can be detected using high-resolution
125 ($\sim 10^2$ m) lidar and radar altimeters such as ICESat and CryoSat-2. Further, comparisons of repeat
126 altimetry profiles at different times of the tidal cycle have been used to identify ephemerally
127 grounded features (Fricker and Padman, 2006).

128        The modulated ice flow of grounded features, such as separate flow centers on ice rises
129 and slower or slightly redirected ice flow over rumples can be detected using interferometric
130 techniques of microwave synthetic aperture radar (SAR) and feature tracking of optical or SAR
131 images (Fig. 1b). SAR interferograms can also reveal variations in tidal flexure associated with
132 the grounding zones, which is particularly useful for identifying small rumples that do not induce

133 shear margins and cannot be visually identified in satellite imagery (e.g., Schmeltz et al., 2001;
134 Rignot, 2002; Scambos et al., 2007). However, delineation of ice-flow centers and divides where
135 surface velocities are small is difficult using ice-flow mapping techniques (e.g., Fig. 1b) and thus
136 the distinction between ice rises and rumples is equivocal. An example of such uncertain
137 characterization is Steershead Ice Rise near Siple Dome (Fig. 3).

## 2.3    Inventory of ice rises and rumples

139 The Appendix contains a satellite-derived inventory of Antarctic ice rises and rumples. The
140 presence of localized ice flow from flow centers or divides is the clearest criterion for
141 distinguishing ice rises from rumples. However, the elevation-based approach described in the
142 Appendix is a more practical way to classify these features. In total, we inventoried 103 isle-type
143 ice rises (group 1), 67 promontory-type ice rises (group 2, including 9 inter-ice-stream ridges),
144 510 ice rumples (group 3), and 24 elevated features with outcrops (group 4).

145       Ice rises and ice rumples exist on every major ice shelf in Antarctica (Fig. 3), but the
146 spatial distribution varies. For example, the Siple Coast has a greater number of relatively large
147 ice rises, whereas the Sulzberger and Abbott Ice Shelves contain many small ice rises and
148 rumples. In contrast, few ice rises and rumples exist near the outlets of major glaciers situated in
149 deep bed troughs (e.g., Byrd Glacier in the Ross Sea Embayment and Recovery Glacier in the
150 Weddell Sea Embayment). Geological constraints on the distribution of ice rises and rumples are
151 discussed in Section 2.5.

## 2.4    Morphology and flow features

153 The new inventory allows evaluation of the geometric characteristics of ice rises and rumples.
154 There is some uncertainty in these attributes because the size of the features is often close to or
155 even smaller than the data resolutions (Appendix). For their lateral extent, isle-type ice rises are
156 typically wider than several kilometers (Table 1), with areas ranging between 10 and $10^3$ km$^2$
157 (Fig. 4a). Promontory-type ice rises have similar dimensions, but defining their upstream extent
158 is often difficult. In contrast, ice rumples rarely extend more than a few kilometers and generally
159 have areas less than ~10 km$^2$. In terms of their vertical extent, most ice rumples are only a few
160 meters higher than the ice-shelf surface, whereas ice rises are typically 10–310 m higher than the
161 adjacent ice shelves and streams (Fig. 4b, Table 1). Nevertheless, ice rises and rumples are of
162 comparable thickness (Fig. 4c), meaning that the bed elevation of most ice rumples is lower than
163 that of a typical ice rise. Except for a few cases, isle-type ice rises have beds below sea level, and
164 most that have been mapped have relatively smooth beds (Fig. 2). The overall shape of ice rises
165 and rumples depends on environmental and physical conditions such as basal shear stress (related
166 to the bed material, e.g., sediments or bedrock), ice flow speed (Fig. 4d), ice thickness (Fig. 4c),
167 wind field, and tidal amplitude, but none of these conditions are clearly distinct between ice rises
168 and rumples.

169       Crests of ice rises are often oriented nearly parallel to the regional ice flow (Fig. 1b) and
170 perpendicular to the prevailing near-surface wind direction (Fig. 2; Lenaerts et al., 2014). Such an
171 orientation suggests a strong geological control associated with erosion of the bed prior to the
172 formation of the ice rises (Wilson and Luyendyk, 2006; Section 2.5). Slope changes associated
173 with the crests are often visible as lineations in satellite imagery (e.g., Henry Ice Rise in Fig. 1a).
174 Ice rises that have been stable for an extended period (Section 4.1) have concave shoulders on
175 both sides of the crest, seen as near-parallel lineations in satellite imagery (Fig. 5; Goodwin and
176 Vaughan, 1995).

177    In order to compensate for higher orographic precipitation (Section 2.7) and maintain in
178    equilibrium, flanks on the windward side are generally steeper than those on the lee side
179    (Vaughan et al., 2004). Flank slopes on most ice rises exceed $\sim 10^{-1}$ degrees (Table 1), which is
180    one to two orders of magnitude steeper than those on the continental ice sheet. Slopes can be
181    even steeper on ice rises located over rough bed topography, and such slope variations in flank
182    are often visible as lineations or variable brightness in satellite imagery (Fig. 5). Except for the
183    largest ice rises (> ~50 km long), the surface topography of ice rises is not well represented by
184    most continent-wide digital-elevation models (DEMs). The surface topography of most ice rises
185    is poorly mapped because of limitations in the spatial sampling of existing satellite altimetry data,
186    particularly along the relatively steep slopes and low latitudes of coastal Antarctica. Nevertheless,
187    accuracy of DEMs is being improved as both radar and laser altimetry techniques are used
188    together (Bamber et al., 2009) and interferometric radar altimetry techniques are refined (Helm et
189    al., 2014).

190    Similarly to the Antarctic Ice Sheet itself, flow features within an ice rise vary greatly
191    from the flow divide to the terminus. Except for regions near the grounding zone, basal melting
192    beneath ice rises is rare because the combination of large SMB (> $\sim 10^{-1}$ m/a) and small thickness
193    (< 1 km) ensures that the bed stays below the pressure melting point (Matsuoka et al., 2012). The
194    ice-flow speed increases gradually towards the grounding zone, but it is less than ~20 m/a in most
195    cases (Fig. 4d, Table 1). Fast-flowing features embedded in ice rises are rare. Exceptions include
196    McCarthy Inlet within Berkner Island in the Weddell Sea Embayment (Fig. 6b), a fast-moving
197    stream within Conway Ice Ridge in the Ross Sea Embayment, and Williamson Glacier within
198    Law Dome in Wilkes Land. These all are located in bed troughs (Fretwell et al., 2013), but it is
199    not clear whether the troughs control fast-flow locations and speeds.

200    Ice flow over ice rumples is much faster than within ice rises (Fig. 4d, Table 1), causing
201    undulating surface topography and heavily crevassed regions (Gudmundsson, 2003). Ice tends to
202    flow more slowly across rumples that are close to larger ice rises or continental grounding zones
203    without glaciers. Flow fields on and around rumples show complicated patterns that reflect the
204    dynamics of the ice shelves and settings of the ice rumples (Fig. 1b).

205    Ice flow near the crests is of special interest because such locations are thought to be
206    particularly suitable for ice coring to obtain minimally disturbed stratigraphic sequences for
207    paleo-environmental interpretations. Except for a zone within a few ice thicknesses of a crest,
208    variations of horizontal velocity with depth are approximately consistent with predictions from
209    laminar flow theory. However, within this crest zone, longitudinal stress gradients are important.
210    Raymond (1983) was the first to complete rigorous analysis of stresses near the crest (ice-flow
211    divide) and he showed that, for ice with non-linear rheology, the horizontal shear strain rate there
212    is less concentrated near the bottom and the downward ice flow is less rapid in comparison to the
213    flanks. This ice-flow regime has important consequences for inferring depth-age relationships at
214    flow divides (Raymond, 1983), and is now generally called the "Raymond effect". As a
215    consequence of the Raymond effect, small shifts in the divide position have a strong effect on the
216    vertical velocity profile (Fowler, 1992). Hindmarsh (1996) examined the dynamic response of ice
217    divides to variations in SMB. Results showed that transient divide motion is most strongly
218    affected by asymmetric variations in SMB halfway between the margin and the divide. Divide
219    migration can also occur from asymmetric changes in fluxes at the margins of an ice divide
220    (Nereson et al., 1998a). These results raise concerns that natural variability in SMB or boundary

221 conditions can cause folding and affect the fidelity of ice-core records extracted from flow
222 divides (Jacobson and Waddington, 2004).

223       Ice-rise response to environmental conditions including climate, relative sea level and
224 ocean circulation occur over a range of timescales. Thus, the morphology and flow regime
225 observed on ice rises today may be: (1) relics of the expanded ice sheet during the last glacial
226 maximum (LGM), (2) transient features that are evolving in response to changes in local ice
227 dynamics and climate, or (3) features that are in steady state with current conditions.

## 2.5       Geological controls on the locations and evolution

### 2.5.1       Continental-shelf morphology and glacial isostatic adjustment

230 The locations of ice rises and rumples are determined primarily by the locations of shallower
231 areas of the continental shelves where the ice shelf can ground (Fig. 6). This pattern is
232 determined by the continental-shelf morphology, which has four key features. First, unlike other
233 areas in the world, the Antarctic continental shelf is down-sloping towards the center of the ice
234 sheet (Arndt et al., 2013). This reverse slope results from the combined effects of long-term
235 glacial erosion (dominant effect) and subsidence (minor effect) owing to the weight of the
236 overlying ice sheet, i.e. glacial isostatic adjustment (Anderson, 1999). Second, faults cut across
237 the continental shelf perpendicular to the coast (transverse faults), which tend to segment the
238 continental shelf and often provide a route for major glacial troughs (e.g., along the western
239 margin of the Antarctic Peninsula). Third, major faults also run parallel to the coast (longitudinal
240 faults) which sometimes manifest as major coast-parallel troughs such as in East Antarctica
241 (Anderson, 1999). Many of these longitudinal faults formed as a consequence of rifting of the
242 Antarctic margin during the break-up of Gondwana in the Jurassic and are consequently long-
243 lived structures (Anderson, 1999). Finally, overlying such tectonic structures, cycles of marine
244 and/or glacial erosion and deposition have left their imprint following the advance and retreat of
245 the ice sheet across the continental shelf during glacial-interglacial cycles (Wilson and Luyendyk,
246 2006).

247       These four features generate a distinctive pattern in the continental-shelf morphology. The
248 inner shelf, closer to the ice sheet, has generally been eroded by ice during periods of greater ice
249 extent, but during times of less ice extent marine deposits can cover the crystalline bedrock. In
250 contrast, the middle and outer shelves are dominated by depositional sequences, primarily of
251 glaciogenic sediment that form shallow banks (e.g., Pennell Bank in the outer Ross Sea; Fig. 6a).
252 Banks may also consist of remnant geological structures that are left upstanding after erosion on
253 either side by paleo-ice streams. Ice rises tend to be located on these banks or on bedrock highs.
254 For example, Roosevelt Island is grounded on an oblong seabed plateau 150–350 m below sea
255 level, about 150-km long and 70-km wide (Fig. 6a). Berkner Island is located on part of an
256 extensive shallow seabed plateau, which may have been completely covered by grounded ice
257 when Berkner Island was larger in the past (Fig. 6b; Bentley et al., 2014). In contrast, its
258 landward side has seabed troughs more than 1000-m below sea level (Fretwell et al., 2013).
259 Longitudinal troughs can create isolated areas of high seabed on the outer parts of the continental
260 shelf.

261       As well as continental-shelf morphology, another key factor controlling the formation of
262 an ice rise or ice rumple is water depth. During glacial-interglacial cycles, global-mean sea level
263 is predominantly governed by changes in global ice volume. However, local water depths will be
264 modulated by glacial isostatic adjustment (GIA), which describes the deformation of the solid

265 Earth and geoid (sea-surface height) in response to regional changes in ice loading (Farrell and
266 Clark, 1976; Whitehouse et al., 2012). The viscous nature of the mantle means that this
267 deformational response can take thousands of years to reach equilibrium. Therefore, following a
268 decrease in ice mass, the subsequent gradual uplift of the seabed combined with lowering of the
269 sea surface due to the decreased gravitational attraction of the smaller ice sheet both act to reduce
270 water depths beneath an ice shelf, potentially leading to the formation of an ice rise.

271 The geology under an ice rise can reflect conditions before the current ice cover. Marine
272 sediment might be present under many ice rises, as suggested by the typical smoothness of the
273 bed (Fig. 2). However, direct sampling has been made only at two sites. Berkner Island (Fig. 6b)
274 has enigmatic well-sorted quartz sand, interpreted to be aeolian in origin but of unknown age
275 (Mulvaney et al., 2007). This sand was recognized as being similar to a widespread unit found in
276 marine cores from the southern Weddell Sea (Rex et al., 1970). Crary Ice Rise in the Ross Sea
277 Embayment (Fig. 6a) is underlain by microfossil-bearing marine sediments (Bindschadler et al.,
278 1990).

279 ### 2.5.2  Mechanisms of ice-rise formation and their geological imprint
280 The previous section outlined how geological and geophysical processes can influence the
281 formation and location of ice rises; namely tectonics, erosion, sedimentation, and GIA. Over
282 shorter timescales, ice rise evolution is mainly controlled by ice dynamics, sea level, and climate.
283 Here, we classify four main ways in which ice rises might evolve. Ice rumples can evolve
284 similarly but presumably over shorter timescales, because most of them are only several meters
285 higher than the surrounding ice shelf (Fig. 4b). Transitions between ice rises and rumples are
286 poorly understood, however (Section 5.3).

287 1. **Long-term stable**

288 Ice rises that were already present as ice rises during periods with an expanded ice sheet are
289 termed here, 'long-term stable' (Fig. 7a). These ice rises remain stable and were not overrun by
290 the ice sheet at least during the last glacial cycle. An example of this type of ice rise is Berkner
291 Island, which remained an independent center of ice flow during the last glacial cycle (Section
292 4.3).

293 2. **Deglacial emergent**

294 Under most circumstances, a retreating ice sheet implies thinning and retreat of the grounded ice
295 and increasing flotation of the ice margin over the continental shelf. However, some ice may
296 remain grounded on a bank of relatively high bed topography resulting in formation of a
297 'deglacial emergent' ice rise surrounded by an ice shelf (Fig. 7b). Ice rises can emerge similarly
298 when the sea level rises (independent of deglaciation); we include such cases in this type as well.
299 Possible examples include Siple Dome and Roosevelt Island (if they were not long-term stable,
300 Section 4.2).

301 3. **GIA emergent**

302 A thinning ice sheet may reach flotation to form an ice shelf, but subsequent post-glacial rebound
303 may lead to re-grounding of the ice on elevated seabed to form an ice rise, here called a 'GIA
304 emergent' ice rise (Fig. 7c). Similarly, sea-level lowering (occurring independently to GIA) can
305 also lead to the emergence of an ice rise; we include such cases in this type as well. A possible
306 example is Bungenstock Ice Rise in the Weddell Sea Embayment (Section 4.3).

307      4. **Glaciological emergent**

308  A climatic or ice-dynamic perturbation of an ice shelf or one of its feeder ice streams and glaciers
309  may cause the ice shelf to thicken and re-ground on shallow areas of the seabed, forming a
310  'glaciological emergent' ice rise (Fig. 7d). Possible examples include Crary and Steershead Ice
311  Rises in the Ross Sea Embayment that grounded in the last millennium (Section 4.2).

312      These four mechanisms of ice-rise formation lead to distinct age-altitude trajectories (Fig.
313  8). These may be recorded in terrestrial glacio-geological records of change such as those based
314  mainly on cosmogenic isotope analysis of erratic boulders deposited on nunataks located
315  upstream of ice rises. The first two mechanisms (cases 1 and 2, Figs. 7a and 7b) cause a
316  progressive thinning of ice with time (declining age-altitude trajectory). The latter two (cases 3
317  and 4, Figs. 7c and 7d) cause a reverse age-altitude trajectory as GIA or climatic/ice-flow effects
318  cause a re-grounding of the ice shelf and subsequent re-thickening. Records resembling the
319  simple declining age-altitude trajectory are widespread in areas upstream of ice rises, for example
320  at the Ford Ranges, upstream of the Sulzberger Ice Shelf ($150^{o}$W) where abundant small ice rises
321  exist today (Fig. 3, Stone et al., 2003). Other examples are found in the Ellsworth Mountains next
322  to the Rutford Ice Stream, which flows between Fletcher Promontory and Skytrain Ice Rise in the
323  Weddell Sea Embayment (Bentley et al., 2010). In contrast, records suggesting a reversal of the
324  age-altitude trajectory have been found on nunataks upstream of former ice shelves, including
325  Larsen A in the Antarctic Peninsula, which formed about 1400 years before present (1.4 ka BP)
326  but collapsed in the past 50 years (Balco and Schaefer, 2013). Such a reverse pattern may be
327  common, particularly if the thickening occurred recently. It is not yet possible to determine the
328  proportion of the different pattern types because evidence has not yet been systematically
329  sampled around the continent and we do not yet have an efficient way to sample subglacial
330  bedrock for exposure-age dating.

331      Concerning the existence of former ice rises, seabed morphology mapped with swath
332  bathymetry has shown an assemblage of ice-rise-related features such as grounding-zone features
333  around the margins of seabed highs or banks that show evidence of radial slow flow (Shipp et al.,
334  1999). However, the origin and timing of these features is not always clear, because shallow
335  areas of the shelf can be modified by iceberg furrows during deglaciation. Shipp et al. (1999)
336  identified several former potential ice-rise locations by interpreting seabed morphology and using
337  seismic evidence of sediment pinch-out against the banks (Section 4.2). Ice rises have likely
338  formed and disappeared throughout many glacial cycles, perhaps having played significant roles
339  in ice-sheet evolution since the formation of the East Antarctic Ice Sheet at the Eocene-Oligocene
340  boundary (34 Ma BP). Ancient ice rises likely had a very different spatial distribution from that
341  of today.

## 2.6    Interactions with adjacent ocean and ice shelf

343  Elevated seabed topography around ice rises and rumples can modify ocean circulation, which in
344  turn can affect basal-melt/freeze patterns in the vicinity of the ice rises and rumples. In this
345  section, we discuss ice-ocean interactions in the context of ice rises and rumples.

### 2.6.1  Oceanography of the Antarctic continental shelf

347  The oceanography of the continental shelves around Antarctica is controlled by the regional
348  atmospheric forcing (Thoma et al., 2008; Dinniman et al., 2012; Zhou et al., 2014), the large-
349  scale thermohaline circulation (Jacobs et al., 1992), and by tides (Makinson and Nicholls, 1999;
350  Joughin and Padman, 2003; Padman et al., 2003).

351     The temperature of ocean water beneath ice shelves varies greatly around the continent. In
352 most of the continental-shelf areas, the ocean temperature is close to the surface-water freezing
353 point (about -1.9 °C) (e.g., Hellmer and Jacobs, 1992; Nicholls et al., 2001; Hattermann et al.,
354 2012). Here, narrow oceanic fronts situated over the continental-shelf break separate these cold
355 shelf waters from deep warm water in the Southern Ocean (Jacobs et al., 1992; Stewart and
356 Thompson, 2015). In the Bellingshausen and Amundsen Seas, weaker fronts are less effective at
357 preventing off-shelf waters from invading the continental shelves, and shelf temperature can
358 reach as high as +1 °C (Jenkins et al., 2010b). Influx of warm deep waters is controlled by how
359 easily the warmer, off-shelf waters can cross the shelf break to enter the continental shelf (Thoma
360 et al., 2008; Nost et al., 2011; Hattermann et al., 2014), and also by how efficiently those waters
361 can be cooled to the surface freezing point (Jacobs and Comiso, 1989; Nost et al., 2011; Årthun
362 et al., 2013). Thus, the oceanographic regime of the continental shelf can be characterized as
363 being dominated either by cross-shelf advection, or by sea-ice production on the continental shelf
364 (Petty et al., 2013).

365 **2.6.2  Ocean circulation beneath ice shelves**
366 Ocean circulation beneath ice shelves is controlled mainly by the topography of the ice-shelf
367 cavity and the regional oceanographic setting (Jacobs et al., 1992; Nicholls et al., 2009). A
368 typical ice-shelf cavity has a two-layer water column in which flow of the upper layer is guided
369 by contours of the ice shelf draft, whereas flow in the deep layer tends to follow contours of
370 seabed elevation. The deep layer is the primary source of heat into the cavity. However, neither
371 the seabed topography under most of the ice shelves nor the ice-shelf geometry are sufficiently
372 well known to permit accurate modeling of ocean-flow paths and heat transfer at the ice-shelf
373 base (Holland and Jenkins, 1999; Makinson et al., 2010). Instead, we consider three widely-used
374 ocean-circulation modes beneath ice shelves: the ice-front mode (mode III in Jacobs et al., 1992),
375 the free-convective mode (mode II), and the ice-pump mode (mode I).

376     The ice-front mode is induced by increased mixing due to upper ocean currents flowing
377 perpendicular to the calving front of the ice shelf. This mode is common to all ice shelves, and
378 typically promotes basal melting of the ice shelf within a few tens of kilometers of the calving
379 front. It is most significant on colder regions of the continental shelf where the basal melt rates
380 are otherwise low, in particular during the summer when the upper water column has been
381 warmed (Zhou et al., 2014).

382     The free-convective mode is driven exclusively by basal melting. Melting produces a
383 strong, buoyant, meltwater-laden (slightly lower salinity) outflow, which drives a compensating
384 inflow at depth resulting in an open overturning circulation. This mode typically occurs beneath
385 ice shelves with high basal melt rates, such as those in the warmer Bellingshausen and Amundsen
386 Sea Embayments.

387     The ice-pump mode is forced mainly by highly saline, continental-shelf water that drains
388 under gravity into areas beneath ice shelves. Since it is formed by sea-ice production, the water
389 flowing into the cavity has a temperature near the surface freezing point (-1.9 °C). As it flows
390 close to the generally landward-deepening seabed (Fig. 2), the freezing point of the saline water
391 increases with the increasing depth by ~0.75 °C/km. The seabed near the grounding zone of the
392 continental ice sheet can be up to 1.5 km below sea level (Fretwell et al., 2013), resulting in a
393 freezing point of ~ -3 °C. Inflowing water at the surface freezing point can therefore melt ice at
394 the ice-shelf base, and the resulting meltwater-rich water, with a temperature below the surface

freezing point, is called ice-shelf water. The ice-shelf water is buoyant and flows up the ice-shelf base. As the hydrostatic pressure reduces with upward motion, the ice-shelf water can become super-cooled with respect to the local freezing point and form ice crystals in the water column. When the flow slows, typically where the slope of the ice-shelf base decreases, the ice crystals can precipitate out and form marine ice, which accretes to the base of the ice shelf. The ice-pump mode is typical of cold-regime continental ice shelves with low basal melt rates.

### 2.6.3  Basal accretion and melting of ice shelves

All three circulation modes described above can contribute to ice-shelf basal melting, and enhanced basal melting is localized near ice-sheet grounding zones (Depoorter et al., 2013; Rignot et al., 2013). However, only the ice-pump mode contributes significantly to accretion beneath ice shelves. This mode effectively pumps ice from deeper regions and fills rifts and basal crevasses with marine ice (Fricker et al., 2001; Khazendar et al., 2001). The accumulated marine-ice layer can make up one third of the ice-shelf thickness (Craven et al., 2009). Such thick marine-ice layers affect ice-column rheology (Lange and MacAyeal, 1986) and ice-shelf integrity by infilling basal crevasses (Glasser et al., 2009).

The free-convective mode dominates ice-ocean interactions in the relatively warm Amundsen and Bellingshausen Sea coasts, while the ice-pump mode dominates in the colder Ross and Weddell Sea Embayments. However, for the numerous smaller ice shelves located over relatively narrow continental shelves, such as the Dronning Maud Land (DML) coast facing the Eastern Weddell Sea, a more complicated picture emerges that is not yet well known. A belt of such ice shelves bounded by ice rises extends along a large stretch of coast. Their calving fronts reach to the continental slope in many cases. Here, the warm deepwater circulating along the shelf break is often only a couple of kilometers away from the calving front, and ice-ocean interactions appear to be controlled by a complex superposition of all three circulation modes (Hattermann et al., 2012; Pattyn et al., 2012a). Deep ocean heat fluxes and associated melt rates near the grounding zones in these environments are controlled by Antarctic slope-front dynamics and are highly variable (Chavanne et al., 2010; Årthun et al., 2012; Hattermann et al., 2014).

The ocean circulation around Antarctica varies over time and space, and changes in large scale climatic forcing may cause regime shifts between different circulation modes. For example, a recent modeling study showed that reduced sea-ice production in a warming world can lead both to a reduction in salinity over the continental shelf and enhanced coupling between wind and ocean currents near the shelf break. Such changes would increase the warm-water inflow and basal melt of the Ronne-Filchner Ice Shelf, which is currently experiencing relatively little melting in the ice-pump mode (Hellmer et al., 2012).

### 2.6.4  Impacts of ice rises and rumples on ice shelves and ocean

Elevated seabed topography and modified ice-shelf shape around ice rises and rumples add more complexity to local ice-ocean interactions. Recent un-grounding of an ice rumple near the grounding zone of the Pine Island Glacier initiated deepening and widening of the ice-shelf cavity around the former rumple, which resulted in a 50% increase in basal melting near the grounding zone (Jenkins et al., 2010a). Ocean-model simulations suggest that this is due to increased separation between warm inflow and cooled outflow as the ice-bed separation has increased (De Rydt et al., 2014). However, processes are complex and the impact of ice rises and rumples on ocean circulation are not well known.

Ice rises and rumples impede nearby ice-shelf flow and affect the stress within ice shelves. The compressive stresses at the upstream margin of an ice rise exert strong buttressing forces on the discharge of inland ice (Thomas, 1979; Jezek, 1984; Doake et al., 1998; Horgan and Anandakrishnan, 2006; Braun et al., 2009; Borstad et al., 2013). In contrast, the tensile stresses at the downstream margin of an ice rise often initiate crevassing and rifting around ice rises and rumples (Figs. 1 and 2), which can propagate and destabilize an ice shelf (e.g., Hulbe et al., 2010; Humbert and Steinhage, 2011).

Ice-shelf flow often produces bands of crevasses and rifts visible in satellite imagery (Limbert, 1964; Swithinbank, 1977; Smith, 1986; Glasser and Gudmundsson, 2012). Theoretical studies suggest that ice-shelf cavities incised upwards into an ice shelf can channelize ice-ocean interactions (Gladish et al., 2012; Sergienko, 2013). Indeed, ice rises and rumples in the Larsen C Ice Shelf produce bands of marine ice downstream (Holland et al., 2009), which affect stability of the ice shelf (Jansen et al., 2013; Kulessa et al., 2014). The overall impact of such structural changes, marine-ice accretion and channelized ocean flow remain poorly understood in the context of ice-shelf dynamics and the role of ice rises and rumples.

## 2.7 Local climate and surface mass balance

The main source of mass input to an ice rise is local snow accumulation. This implies that local surface mass balance (SMB) strongly controls ice-rise evolution. The topographic signature of an ice rise on a relatively flat ice shelf impacts the local and regional SMB pattern over ice shelves (Lenaerts et al., 2014). However, owing to their small size, individual ice rises are not well represented in most atmospheric-circulation models, which hampers modeling of the magnitude and spatial patterns of SMB across ice rises and over adjacent ice shelves.

Two distinct wind systems are in operation in coastal Antarctica. One is the downslope katabatic winds from the Antarctic Plateau towards the coast. These follow large-scale topography and are thus usually directed from south to north, but slightly deflected to the west by the Coriolis effect (Van Lipzig et al., 2004). It results in surface winds prevalently from the southeast in Antarctica. The other wind is related to synoptic-scale storms, which transports moist air inland (e.g., Gorodetskaya et al., 2013; Lenaerts et al., 2014). As the moist air rises on the windward side of ice rises, it condenses resulting in precipitation. The pattern of SMB around an ice rise is dominated by orographic precipitation on the upwind side during synoptic storms (Fig. 2).

In-situ observations and regional climate models indicate that SMB on the windward side of ice rises can be 2–5 times higher than that on the adjacent ice shelf (Fernandoy et al., 2010; Lenaerts et al., 2012; Drews et al., 2013). On the downwind side of the ice rise, however, downslope flow warms and dries the air adiabatically; here SMB is less than on the ice shelf (Lenaerts et al., 2014). Also, anomalously low SMB can occur near the crest, as a result of wind erosion (Lenaerts et al., 2014; Drews et al., 2015). SMB patterns are also affected by small variations in the wind field and associated drifting snow (King et al., 2004; Lenaerts and van den Broeke, 2012). Other topographic effects include (1) horizontal divergence of the wind field on the upwind side, (2) strong down-slope acceleration on the downwind side, (3) increased snow erosion associated with the high wind speeds, and (4) increased snow sublimation by relatively dry air on the downwind side of an ice rise. For example, spatial patterns of SMB observed over Lydden Ice Rise in the Brunt Ice Shelf (20$^{o}$W) are reproduced well with a simple airflow model coupled to a blowing snow transport parameterization, under the assumption that precipitation variations across the ice rise are negligible (King et al., 2004).

483     Observations of SMB over ice rises are complicated by significant spatial variations in the
484     near-surface density and vertical strain. First, consider density. Snow density is often assumed to
485     be spatially uniform and SMB is assumed to be proportional to observed stake heights. However,
486     analysis of shallow (3-m long) firn cores across three ice rises in the Fimbul Ice Shelf indicate
487     that variations in surface snow density over an ice rise can exceed 35% (J. Brown and K.
488     Matsuoka, unpublished data). This variation results in a discrepancy of calculated SMB from
489     stake measurements by up to ~20% when compared with calculations based on the mean of all
490     density measurements. Assuming uniform density is also problematic when estimating SMB
491     using near-surface radar reflectors (assumed to be isochrones), because the density affects radio-
492     wave propagation speed and hence the calculation of depth to the reflector. Spatial variations in
493     vertical strain are also a concern because they violate the so-called "shallow-layer
494     approximation" (i.e. the local layer thickness is proportional to the SMB for the corresponding
495     periods (Waddington et al., 2007)). This assumption is often used to derive SMB but it can be
496     particularly problematic over ice rises owing to the combination of relatively small ice thickness
497     and large SMB (Vaughan et al., 1999; Drews et al., 2015), and basal melting near the grounding
498     zone (Catania et al., 2010; Matsuoka et al., 2012).

## 3.     Impacts of ice rises and rumples on ice-sheet dynamics

500     Ice rises and rumples interact with the seabed (Section 2.5), atmosphere (Section 2.7), ocean, and
501     ice shelves (Section 2.6.4), and feedbacks with these components can alter the dynamics and
502     morphology of ice rises and rumples (Section 2.4). Ultimately, these feedbacks especially those
503     within ice shelves cause buttressing, which regulates the grounding-zone position and reduces
504     fluxes from the ice sheet (Gagliardini et al., 2010). However, only a few studies have evaluated
505     the interplay between ice rises, grounding zones, and evolution of the ice sheet. Prognostic
506     modeling studies have so far been limited to synthetic cases.

507     Thomas (1973a; 1973b) used measurements of strain rates to calculate the buttressing
508     exerted by the MacDonald Ice Rumples in the Brunt Ice Shelf and concluded that the buttressing
509     effect is inversely proportional to the distance from the ice rumples. Buttressing from Crary Ice
510     Rise reduce the horizontal spreading rates in front of the Mercer and Whillans Ice Streams by
511     several orders of magnitude compared with that which would occur without the ice rise (Thomas
512     and MacAyeal, 1982). The resistance exerted by Crary Ice Rise accounts for about 50% of the
513     buttressing on the Whillans Ice Stream (MacAyeal et al., 1987). Using a finite element model,
514     Schmeltz et al. (2001) showed that ice rises reduce the discharge from Pine Island Glacier.
515     Similar impacts were found for Bawden and Gipps Ice Rises in the Larsen C Ice Shelf; these two
516     small ice rises near the calving front slow the flow of the ice shelf (Borstad et al., 2013). Current
517     ice-flow models cannot replicate observed pattern of flow of ice shelves around ice rises and
518     rumples that are not charted in the Bedmap2 data but visible in satellite imagery (Fürst et al.,
519     2015).

520     The net effect of an ice rise on the flow of grounded ice depends on the ice rise's location
521     within an ice shelf. For example, ice rises in a well-protected inlet of the Ronne-Filchner Ice
522     Shelf have very small influences (Schmeltz et al., 2001). Similarly, the disappearance of an ice
523     rumple from Thwaites Glacier's floating ice tongue increased flow speeds at the grounding zone
524     on either side of the ice tongue, but the maximum speed of the tongue remained unchanged
525     (Rignot, 2008). Furthermore, a model study showed that potential un-grounding of a local
526     grounding feature near the front of the slowly-moving eastern part of the Thwaites glacier tongue
527     seems to have a little influence on mass-balance projection of the glacier (Joughin et al., 2014).

528   Favier and Pattyn (2015) were the first to model the progression from a promontory-type ice rise
529   to an isle-type ice rise as the grounding zone retreats beyond a locally-elevated seabed (a
530   seamount). The presence of an ice rise affects the timing of deglaciation by exerting buttressing
531   on the ice sheet, but in steady state grounding-zone positions only slightly differ when the
532   seamount and associated ice rise are present or absent. They point out that promontory-type ice
533   rises are transient features during the deglaciation, whereas isle-type ice rises are more stable. In
534   steady state, the ice shelf seaward of the ice rise is much thinner than on the landward side,
535   consistent with an observation (Fig. 2). This may explain why many isle-type ice rises limit the
536   seaward extent of the ice shelf (Fig. 3). Model experiments by others over glacial-interglacial
537   cycles have also demonstrated that ice rises play an important role both in the growth and
538   collapse of the ice sheets (Pollard and DeConto, 2009; 2012). Although it is clear that ice rises
539   influence the flow of the grounded ice, the controls are complicated, and depend on the shape and
540   distribution of ice rises and seamounts.

541   Isle-type ice rises and ice rumples play a role in modulating the development of a marine-
542   ice-sheet instability (MISI). A MISI occurs when the initial thinning and retreat of the grounding
543   zone causes thinning and floating of the upstream part of the ice sheet on an inland-deepening
544   bed (Weertman, 1974; Schoof, 2007). Goldberg et al. (2009) first examined the influence of a
545   local grounding on a seamount, and found that its presence can stabilize MISI-induced
546   grounding-zone retreat, and in fact, perhaps reverse the process, resulting in unstable advance.
547   Bradley et al. (2015) invoke this process to explain GPS-observed solid Earth deformation in the
548   Weddell Sea Embayment (Fig. 6b), concluding that the grounding zone must have retreated
549   upstream of Bungenstock Ice Rise during the late Holocene and then subsequently re-advanced to
550   its current unstable position following GIA-induced re-grounding of the ice shelf landward of the
551   ice rise. Favier et al. (2012) examined the effects of ice-rumple emergence by forcing a model
552   with an abrupt decrease in sea level. In this case, the ice shelf grounded on a seamount, producing
553   first an ice rumple. The buttressing decreased the ice-shelf speed and the ice-sheet's grounding
554   zone advanced until it merged with the rumple. Once the ice rumple had been subsumed by
555   grounded ice, the grounding zone did not revert back to its original position even if the sea level
556   was increased back to the initial value. Despite these advances, models have not yet produced a
557   steady configuration where ice rises or rumples exist within ice shelves, except for a recent work
558   on a stable isle-type ice rise during deglaciation (Favier and Pattyn, 2015).

559   Additional model experiments by Schmeltz et al. (2001) showed that an ephemeral ice
560   rumple during low tides has only a small influence on the flow of the ice shelf. The results
561   suggest that thickening beyond a critical value (perhaps sufficient to maintain grounding over
562   tidal cycles) is necessary to have a significant buttressing. However, conditions for sustained
563   grounding are a threshold problem, which is poorly understood. None of the above-mentioned
564   model experiments were designed to examine impacts of ice rises and rumples separately. Also,
565   the model used here is diagnostic, not transient, which is not fully capable to capture the effects
566   of grounding zones. Additional work is needed to understand the details of the impact of ice rises
567   and rumples on grounding-zone dynamics.

## 4.      Records and dynamic roles of ice rises during Holocene

569   Ice rises and rumples have impacted on the Holocene deglaciation of Antarctica. The
570   glaciological imprints of such changes from ice rumples are advected downstream, but those
571   from ice rises remain locally in their thermal structure (Bindschadler et al., 1990) and englacial
572   stratigraphy (Conway et al., 1999). Owing to the relatively thin ice (ice thickness $H = 220 — 640$

573     m; Table 1) and large SMB around the Antarctic coast ($b$ > ~0.1 — 0.3 m/a; Van de Berg et al.
574     (2006) and Lenaerts et al. (2014)), the characteristic ice-flow timescale $T$ (= $H/b$; Cuffey and
575     Paterson (2010)) of ice rises is typically several thousand years or shorter. Thus, ice rises can
576     potentially retain an imprint of past evolution for several millennia. Furthermore, as most ice
577     rises are frozen to their beds (except near the grounding zone), ice near the bed can be much older
578     than the several millennia, potentially well beyond the LGM (Mulvaney et al., 2007; Bertler et
579     al., 2014; Mulvaney et al., 2014). Glaciological imprints over shorter periods (less than a
580     millennium) can also be seen in the shape of satellite-observed flow stripes on the ice shelf.
581     These features generated near ice rises and rumples are then advected downstream by flow of the
582     ice shelf (Fahnestock et al., 2000) and have been used to infer temporal changes in the relative
583     contributions of adjacent ice-flow units downstream of ice rises (Hulbe and Fahnestock, 2007).

584         In this section, we first describe the physical mechanisms that generate englacial
585     stratigraphy, and how they can be used to constrain evolution of ice rises and their vicinities
586     (Section 4.1). We then review current knowledge of Holocene deglaciation in four sectors of
587     Antarctica, emphasizing the records and dynamic roles of ice rises (Sections 4.2–4.5). The lesser-
588     explored regions that constitute half of the Antarctic coast are briefly discussed in Section 4.6.

## 4.1   Constraints from englacial stratigraphy

590     Dated ice cores from ice rises can be used as dipsticks to extract histories of ice thickness. The
591     thickness of an annual layer (in ice equivalent, the derivative of the depth-age relationship)
592     depends not only on its initial thickness (the annual SMB, when it was deposited) but also on the
593     cumulative vertical strain since it was deposited. Therefore, when the history of SMB can be
594     determined independently, the history of ice thickness can be inferred (Waddington et al., 2005).

595         Radar-detected englacial stratigraphy (Fig. 2) also provides a powerful constraint on the
596     evolution of ice rises. The shapes of the observed reflectors (assumed to be isochrones) are
597     replicated using numerical ice-flow models for several hypothetical cases, and comparison to
598     observed features is used to judge the likelihood of each case. Histories of ice flow can be
599     extended further back in time when the radar reflectors can be dated by tracking them back to an
600     ice-core site.

601         For ice rises, modeling efforts focus on the near-crest or near-summit region (ice-flow
602     divide). The nearly flat surface in the divide vicinity makes the driving (gravitational) stress
603     applied to that ice much smaller than that applied to flank ice, and the main stress is the
604     longitudinal stress caused by the flank ice tugging on the divide ice. Owing to Glen's power flow
605     law, ice near the bed within two to three local ice thicknesses from the divide is much stiffer than
606     the ice at a corresponding elevation in the flank, which impedes downward flow. This divide-
607     specific flow characteristic was predicted by Raymond (1983) and is frequently called the
608     "Raymond effect". When certain conditions (outlined below) are satisfied, the Raymond effect
609     often causes divide ice of a given age to be at shallower depths than the flank ice, causing
610     "Raymond (upward) arches" in the isochronous ice stratigraphy (Figs. 2 and 9a). Raymond et al.
611     (1995) first observed local upward radar reflectors beneath the divide of Siple Dome, which can
612     be associated with a local low in SMB and/or local flow regime at a divide (i.e. Raymond effect).
613     Nereson et al. (1998b) used it to analyze migration of the divide, assuming that it is a proxy of the
614     divide position in the past regardless of its cause. Vaughan et al. (1999) demonstrated that these
615     causes can be distinguished using a simplified ice-flow model; a persistent local low in SMB
616     causes arch amplitudes that increase with depth linearly, while amplitudes of Raymond arches
617     increase quadratically with depth. Using this method, upward arches found at 20-80 m depths in

618    Fletcher Promontory were diagnosed as Raymond arches (Vaughan et al., 1999). Conway et al.
619    (1999) first analyzed the depth profile of the Raymond-arch amplitudes to determine the onset of
620    timing and thinning at Roosevelt Island.

621    Raymond arches become distinctly visible in radargrams after one characteristic time
622    period *T*, and reach a steady state after a few *T* (Martin et al., 2009b). The amplitude of the
623    Raymond arches increases from the top to about two thirds of the ice thickness, and decreases
624    from there to the bottom of the divide (Fig. 9b). The shape of (the stack of) Raymond arches has
625    been used to infer the onset timing of divide flow and ice thickness changes (Conway et al., 1999;
626    Martin et al., 2006), divide migration (Nereson and Waddington, 2002), and stochastic variations
627    in divide position (Hindmarsh, 1996; Martin et al., 2009b). However, the shape can also be
628    modified by (1) the spatial SMB patterns (Nereson et al., 2000; Nereson and Waddington, 2002;
629    Drews et al., 2013; 2015), (2) the temperature profile through the ice column and geothermal flux
630    (Hvidberg, 1996; Nereson and Waddington, 2002), (3) variations in ice rheology (Martin et al.,
631    2006; Pettit et al., 2007; 2011) and (4) basal sliding (Pettit et al., 2003; Martin et al., 2009b). In
632    fact, Raymond arches will not form under conditions of strong basal sliding (Pettit et al., 2003),
633    but vertically-oriented alignments of ice crystals should increase the arch amplitude (Pettit et al.,
634    2007; Martin and Gudmundsson, 2012).

635    R.C.A. Hindmarsh and G.H. Gudmundsson observed radar-detected complex arches in
636    the bottom one third of the ice beneath the divides of Fletcher Promontory and Kealey Ice Rise
637    during the 2005-6 Antarctic field season. The stratigraphy includes a combination of two
638    anticlines; one is like Raymond arches, and the other is a downward curving fold (syncline) in the
639    central part (Fig. 9a). Also, the tail of the larger Raymond arches often shows small flanking
640    synclines (Fig. 1 in Hindmarsh et al., 2011). Parrenin and Hindmarsh (2007) demonstrated that
641    flanking synclines can arise as a consequence of sharp horizontal changes in the ice viscosity.
642    Martin et al. (2009a) argued that these synclines in the central and flank parts of the Raymond
643    arches can form as a result of the development of crystal alignments under stress configurations
644    unique to the divide (i.e. Raymond effect), so hereafter we call this stratigraphy "double-peaked
645    Raymond arches". Martin et al. (2009a) also showed that the development of crystal alignments
646    could also explain the concave shoulders observed in the surface topography near some divides,
647    which are visible as two near-parallel lineations in satellite imagery (Fig. 5; Goodwin and
648    Vaughan, 1995). It takes at least $1T$ to develop concave shoulders and $2T$ to develop the double-
649    peaked Raymond arches (Martin et al., 2009a). The different time scales might explain why near-
650    parallel satellite lineations are visible on Korff Ice Rise (Fig. 5a) but radar-detected stratigraphy
651    shows single-peaked Raymond arches (J. Kingslake, unpublished data).

652    Many Raymond arches in ice rises have not fully responded to Holocene deglaciation,
653    because a steady state is reached progressively later at greater depths, and thus the entire stack of
654    the Raymond arches reaches steady state only after ~$10T$ in anisotropic ice (Martin et al., 2009a).
655    Where the Raymond arches have not yet reached steady state, their shape is affected by the
656    evolution of the ice mass (Nereson et al., 1998a; 1998b; Nereson and Raymond, 2001). The
657    interpretation of histories of ice dynamics from the shape of the Raymond arches is not always
658    unequivocal. Ambiguities come from uncertainties in the flow law (i.e., Glen's Index, Drews et
659    al., 2015), the evolution of alignments of ice crystals (Martin and Gudmundsson, 2012), and
660    SMB history (Waddington et al., 2005).

661    Vertical velocities in ice rises have been measured directly using phase-sensitive radar
662    (Gillet-Chaulet et al., 2011; Kingslake et al., 2014) or borehole strain measurements (Pettit et al.,

663  2011), which allows one to constrain Glen's Index and assess the evolution of the ice rises more
664  reliably from the shape of the Raymond arches. Nevertheless, Glen's Index changes with time, as
665  the crystal alignments change. The Law Dome ice core shows that ice-crystal alignments can be
666  variable even in the dome of the ice rise (Wang et al., 2002).

667  Raymond arches have been found at all ice rises investigated so far, except for Conway
668  Ice Ridge in the Ross Sea Embayment (see Section 4.2). Therefore, although Raymond arches are
669  relatively common on ice rises, they have not been observed beneath the continental divides of
670  the Antarctic Ice Sheet (Neumann et al., 2008; Fujita et al., 2012). This absence may be explained
671  by a combination of long characteristic time (10-20 ka for West Antarctica and more than 100 ka
672  for East Antarctica), basal melting owing to small SMB and thick ice (Pattyn, 2010), and possible
673  divide migration during the Holocene beyond the lateral range of the Raymond effect, which is
674  only a small fraction (1-2 %) of the flowline from the divide to the coast. In contrast, on ice rises,
675  a combination of thin ice and large SMB keep the bed frozen, creating a significant Raymond
676  effect over a relatively long range (10–15% of their flow line). Also, characteristic times are at
677  least one order of magnitude shorter than the continental divides. These conditions make the
678  Raymond arches in ice rises more persistent and useable in constraining regional evolution.

## 4.2   Ross Sea

680  Onshore and offshore studies show that an expanded, grounded ice sheet occupied the Ross Sea
681  during the LGM, which raises the question: did the Ross Embayment have ice rises during the
682  LGM? On the western continental shelf, north of Ross Island, troughs between four prominent
683  banks (Ross, Pennell, Crary, and Mawson; Fig. 6a) show evidence of mega-scale glacial
684  lineations, grooves, and grounding zone wedges, but relatively few glacial geological features
685  occur on the banks themselves. One explanation is that these banks supported ice rises that were
686  frozen to the bed (Shipp et al., 1999). It is thought that there were ice rises during an early retreat
687  of the ice sheet but that the ice rises disintegrated when the Ross Ice Shelf retreated farther south
688  in the early Holocene (Anderson et al., 2014). Early glaciological reconstructions (Hughes, 1973;
689  Thomas, 1973b; Whillans, 1973; Thomas, 1979) recognized the possibility of such pinning points
690  and their effect on stabilizing (or destabilizing) the expanded ice sheet.

691  Numerous ice rises (including inter-ice-stream ridges) and ice rumples also exist in the
692  Ross Ice Shelf today (Fig. 3). Roosevelt Island, which is near the present ice-shelf calving front
693  in the eastern Ross Embayment, provides a strong constraint on the deglaciation history of the
694  region. Depth profiles of radar-detected Raymond arches indicate that divide flow started 3 ka
695  BP, with the implication that the grounding line retreated past Roosevelt Island at this time
696  (Conway et al., 1999; Martin et al., 2006). Preliminary results from a full-depth ice core drilled
697  on the divide by the RICE consortium indicate a continuous record extending back 30–40 ka BP
698  (Bertler et al., 2014).

699  Siple Dome, an inter-stream ridge between Kamb and Bindschadler Ice Streams in the
700  central Ross Embayment, has been the site of extensive glaciological investigations, including a
701  1004-m-long ice core to the bed (Taylor et al., 2004). Depth profiles of age (Brook et al., 2005)
702  and borehole temperature (MacGregor et al., 2007) have been used to infer thinning of ~350 m
703  about 14–15 ka BP (Price et al., 2007). The shape of radar-detected stratigraphy across the dome
704  shows that divide flow started 3 ka BP, and the divide started migrating northward 2.5 ka BP,
705  likely because of relative changes in the activity of the bounding ice streams (Nereson and
706  Raymond, 2001). Raymond arches in nearby Engelhardt and Shabtaie Ice Ridges have also been
707  migrating northward over the past few thousand years; the implication is that the surface

708 elevation of ice streams to the south have been decreasing during this period (Nereson and
709 Raymond, 2001). In contrast, radar surveys across Conway Ice Ridge between Mercer and
710 Whillans Ice Streams do not show evidence of Raymond arches. Rather, the englacial
711 stratigraphy is highly disturbed and folded, suggesting that the ice ridge has been over-run by fast
712 moving ice in the recent past (Conway et al., 2005).

713 Unlike Siple Dome, Crary and Steershead Ice Rises are not relics of the expanded LGM
714 ice sheet, but instead they have emerged within the last millennium owing to increased discharge
715 from Kamb and Whillans Ice Streams (MacAyeal et al., 1987; Bindschadler, 1993). Evidence
716 from cooling trends measured in two boreholes on Crary Ice Rise have been used to estimate that
717 grounding occurred ~1.1 ka BP at one site and 580 years ago at the other site (Bindschadler et al.,
718 1989; 1990). Flow stripes preserved in the Ross Ice Shelf contain a rich history of interactions
719 between ice stream, ice shelf, and ice rise over the past millennium (the time it takes for shelf ice
720 to transit to the ocean). Numerical modeling shows (i) grounding of Crary Ice Rise ~1 ka BP,
721 followed by stagnation of Whillans Ice Stream 150 years later and recommencement of streaming
722 flow ~450 years ago; (ii) grounding of Steershead Ice Rise ~200 years ago followed by
723 stagnation of Kamb Ice Stream ~50 years later (Hulbe and Fahnestock, 2007; Catania et al.,
724 2012). This rich history of interactions between ice rise evolution and slow-downs of nearby ice
725 streams has the potential to elucidate controlling processes near grounding zones.

## 4.3  Weddell Sea

727 Offshore studies show that the Weddell Sea Embayment had a thin cover of grounded ice during
728 the LGM, sloping very gently from the interior to the margin at the continental shelf break when
729 it had its maximum extent (Hillenbrand et al., 2013). Marine-sediment records and cosmogenic
730 isotope dating of outcrops (Bentley et al., 2010) show similar timings of ice-sheet retreat (~15 ka
731 BP). This embayment has far fewer outcrops suitable for geological surveys than the Ross Sea
732 Embayment, and offshore surveys in the Weddell Sea are often restricted by unfavorable sea-ice
733 conditions. Glaciological imprints on ice rises therefore provide important information about
734 Holocene deglaciation of the region.

735 Today, the Weddell Sea Embayment contains a diverse population of ice rises (Figs. 1, 3,
736 6b). Berkner Island, Korff and Henry Ice Rises are surrounded entirely by the Ronne-Filchner Ice
737 Shelf. Fowler Peninsula, Fletcher Promontory, and Skytrain and Bungenstock Ice Rises are inter-
738 ice-stream ridges constituting part of the continental grounding zone, whereas Kealey Ice Rise is
739 an inter-ice-stream ridge adjacent to tributaries of ice streams, located landward of the grounding
740 zone. Radar surveys have been carried out on Berkner Island, Fletcher Promontory (Vaughan et
741 al., 1999; Martin et al., 2009a; Kingslake et al., 2014), Kealey Ice Rise (Martin et al., 2014),
742 Bungenstock Ice Rise (Siegert et al., 2013), Fowler Peninsula, and Korff, Skytrain, and Henry Ice
743 Rises (J. Kingslake, unpublished data). Raymond arches in the radar stratigraphy have been
744 analyzed at Berkner Island (Hindmarsh et al., 2011), Fletcher Promontory (Vaughan et al., 1999;
745 Hindmarsh et al., 2011), and Kealey Ice Rise (Martin et al., 2014). Initial analyses show no clear
746 evidence of Raymond arches in Henry Ice Rise, and Korff Ice Rise (Fig. 5a) is unique in that
747 near-parallel lineations near the crest are visible in satellite images, but radar-detected
748 stratigraphy shows single-peaked (rather than double-peaked) Raymond arches (J. Kingslake,
749 unpublished data).

750 Deep ice cores have been drilled at Berkner Island (948-m long to the bed; Mulvaney et
751 al. (2007)) and Fletcher Promontory (654-m long to the bed; Mulvaney et al. (2014)). The
752 Berkner Island core suggests that the basal ice may be older than 120 ka and that the LGM-

753 Holocene transition is 300–350 m above the bed (Mulvaney et al., 2007). Berkner Island has
754 probably been persistent, constituting an independent flow divide during the LGM, though it
755 remains unknown whether Berkner Island was an isle- or promontory-type ice rise. Initial
756 analysis of the ice core from Fletcher Promontory also suggests that it will provide a similarly
757 detailed record extending back at least 100 ka BP (Mulvaney et al., 2014). These two ice cores
758 show that long histories of climate and ice dynamics can be preserved in ice rises.

759 Radar stratigraphy collected on Berkner Island, Fletcher Promontory and Kealey Ice Rise
760 all suggest divide positions unchanged over an extended period. Kealey Ice Rise has double-
761 peaked Raymond arches and corresponding near-parallel satellite lineations, which suggest that
762 the divide position has been stable over the past 3 ka, although more recent reorganization of
763 flow in the last century cannot be excluded (Martin et al., 2014). Berkner Island and Fletcher
764 Promontory flow centers are triple junctions of ice crests (Hindmarsh et al., 2011). Analysis of a
765 radar survey across the Berkner Island triple junction shows one strong Raymond arch that has
766 been in steady state since it started forming ~4 ka BP but arches on the other ridge are muted.
767 The survey across the Fletcher Promontory triple junction shows a clear set of arches that suggest
768 the summit occupied this position ~5 ka BP, and has been thinning with a mean rate of 0.1 m/a.
769 In addition, a set of well-developed, double-peaked Raymond arches exists about 3 km from the
770 current summit of Fletcher Promontory. It is likely that the arches formed owing to development
771 of ice-crystal alignment, but the location and shape of the arches is not completely explained by
772 current understanding of the physics and timescales of processes (Hindmarsh et al., 2011).

773 In contrast, Bungenstock Ice Rise has experienced significant changes in its flow regime
774 over the late Holocene (Siegert et al., 2013). Radar-detected stratigraphy shows surface
775 conformable, undisrupted layering in the upper half of the ice column, but highly deformed and
776 buckled layering in the lower half. The stratigraphic sequence suggests that the older ice was
777 deposited upstream of the present-day ice rise and was deformed by enhanced flow, while the
778 younger undisrupted layers were deposited after the ice rise grounded (Siegert et al., 2013).
779 Bungenstock Ice Rise could have developed either as a promontory-type ice rise during the
780 grounding-zone retreat, or initially as an emergent isle-type ice rise before transitioning to a
781 promontory type as the grounding zone advanced further. Bradley et al. (2015) present GIA data
782 and modeling results that support the grounding zone re-advance hypothesis.

## 4.4 Antarctic Peninsula and Amundsen Sea
784 The Antarctic Peninsula and Amundsen Sea regions have been undergoing deglaciation since the
785 LGM, generally from outer-to-inner regions and north-to-south (Heroy and Anderson, 2007).
786 Numerous ice rises in this region presumably have strong controls on the regional deglaciation
787 pattern. In recent decades, glaciers and ice shelves around the Antarctic Peninsula and along the
788 Bellingshausen Sea Coast (bounded by the Antarctic Peninsula and Pine Island Bay) are changing
789 rapidly (Vaughan et al., 2003; Thomas et al., 2008), with several shelves in the Antarctic
790 Peninsula collapsing or thinning in response to atmospheric warming (Cook and Vaughan, 2010)
791 or thinning due to basal melting (Pritchard et al., 2012).

792 Satellite imagery shows two near-parallel lineations (similar to those shown in Fig. 5)
793 near the crest of 23 ice rises in this region (Fig. 10). Modest ice thickness (population statistics $H$
794 $\approx 490 \pm 200$ m; Fretwell et al., (2013)) and very high SMB ($b \approx 0.92 \pm 0.48$ m/a water equivalent;
795 Arthern et al. (2006) and van den Broeke et al. (2006)) indicate that the characteristic time scales
796 $T$ are less than 500 years for 12 ice rises and 500–1000 years for six ice rises. The short

797  characteristic times and their proximity to the coast make them sensitive indicators of recent
798  climate- and ocean-driven dynamic change.

799  Detailed ground-based radar surveys have been conducted over four ice rises: Adelaide
800  Island (or Fuchs Piedmont, Martin et al., 2009a; Kingslake et al., 2014), King George Island
801  (Blindow et al., 2010), Latady Island, and Monteverdi Peninsula (H. Pritchard, unpublished data).
802  Also, airborne radar surveys were flown during the British Antarctic Survey's GRADES-IMAGE
803  project on two other ice rises. King George Island has single-peaked Raymond arches, while all
804  the other five ice rises have well-developed, double-peaked Raymond arches (Fig. 9). The time
805  scale for formation of double-peaked arches is $2T$ or longer (Martin et al., 2009a). An implication
806  is that conditions at these sites have been largely unchanging at least for several centuries.
807  Furthermore, any change in the dynamics must have been very recent because more sustained
808  change would remove the architecture of the Raymond arches.

809  Raymond arches detected on Adelaide Island are offset from the current topographic
810  divide (Martin et al., 2009a). Ice-flow modeling shows that this offset is unlikely to be a steady-
811  state asymmetry caused by sloping bed or a gradient in SMB. Instead, it is likely to have been
812  caused by a recent and anomalous change in ice flux across one of the margins of the island, but
813  the change is too recent to have removed the existing architecture or to have caused a new stack
814  of arches to form beneath the current divide position. The response time of divide location to a
815  flux perturbation at the margin is $\sim T/16$ (Hindmarsh, 1996), which is ~25 years in this case.
816  Additional work is needed to constrain the timing of changes more accurately and to investigate
817  signals of changes across other divides in this region.

## 4.5  Dronning Maud Land

819  Glacial-interglacial variations of the ice-sheet margin in Dronning Maud Land (DML; 20° W -
820  45° E) are probably smaller than most other regions owing to its close proximity to the
821  continental-shelf break (Mackintosh et al., 2013). Currently the DML coast consists of 1500-km
822  of ice shelves, fed by outlet glaciers and punctuated by numerous ice rises (Fig. 3). Most ice
823  shelves extend less than 100 km from the grounding zone to the calving front, which is close to or
824  even beyond the continental-shelf break (Arndt et al., 2013). The area of ice shelves in this region
825  decreased by 6.8% between 1963 and 1997, mostly in regions without ice rises and rumples near
826  the calving front (Kim et al., 2001). This observation supports the hypothesis that ice rises
827  generally stabilize ice shelves.

828  So far only seven of ~30 inventoried ice rises in DML have been investigated. These are
829  Søråsen Ridge (10° W; A. Winter and D. Steinhage, pers. comm.), Halvfarryggen Ridge (7° W;
830  Drews et al. (2013)), three ice rises near the Fimbul Ice Shelf (Blåskimen Island, Kupol
831  Moskovskij, and Kupol Ciolkovskogo; Norwegian Antarctic Research Expeditions), an unnamed
832  ice rise at 24° E (Matsuoka et al., 2012; Pattyn et al., 2012a), and Derwael Ice Rise (26° E; Drews
833  et al. (2015)) both in the Roi Baudouin Ice Shelf. In addition, field and remote-sensing studies are
834  ongoing at ice rumples in the Roi Baudouin Ice Shelf (Belgian Antarctic Research Expeditions).
835  Many ice rises in DML have topographic ridges roughly perpendicular to the prevailing wind
836  direction, so their influence on the regional pattern of SMB is strong (Lenaerts et al., 2014).

837  All seven ice rises have distinct Raymond arches, except for an unnamed ice rise at 24° E,
838  which nevertheless has distinct arches beneath its crest but the undulated bed there prevents
839  conclusive interpretation of its cause. Halvfarryggen Ridge has double-peaked Raymond arches
840  (Fig. 9), and corresponding near-parallel lineations are visible in satellite imagery (Fig. 5b).

841  Model results indicate that the divide position has been steady for at least 2.7–4.5 ka, a time
842  period necessary to generate these features with anisotropic ice flow (Drews et al., 2013). Seismic
843  reflections from within the ice rise indicate developed alignments of ice crystals (Hofstede et al.,
844  2013). Radar data collected at three ice rises in the Fimbul Ice Shelf (Fig. 2) are being examined
845  in terms of temporal changes in SMB patterns and differential variations of ice-shelf thicknesses
846  adjacent to the ice rises.

847  Derwael Ice Rise deflects ice-shelf flow fed by West Ragnhild Glacier, one of the three
848  largest glaciers in DML (Callens et al., 2014). The amplitudes of the observed Raymond arches
849  fit best with models when it is assumed that the ice rise has been in a steady state or thinned
850  slightly (~3 cm/a) over the past ~3.4 ka (Drews et al., 2015). The 120-m-long ice core drilled at
851  the summit by the Belgian Antarctic Research Expeditions will constrain a climate record for the
852  past century.

## 4.6   Other less-studied regions

854  The four regions described above constitute only about half of the Antarctic coast, and ice rises
855  and rumples in the other half remain largely unexplored. Here, we review our knowledge of this
856  unexplored region, moving eastward from DML.

857  There are fewer ice rises in Enderby Land (~50° E), Wilhelm II Land (~90° E), and
858  Wilkes Land (~120° E) than in the above-mentioned regions, though there are many ice rumples
859  in Wilheim II Land and Wilkes Land (Fig. 3). Here, ice-shelf extent is smaller than other regions
860  in Antarctica, which partly explains the smaller population of isle-type ice rises. Only Mill Island
861  (101° E) at the calving front of the Shackleton Ice Shelf and Law Dome (113° E) have been
862  studied in these sectors. Inverse modeling using a 120-m-long borehole temperature profile
863  acquired on Mill Island indicates surface temperature warming of 0.37° K per decade over the
864  past 30 years (Roberts et al., 2013). The warming is attributed to changes in climate. The calving-
865  front positions of many ice shelves in Wilkes Land, including Mill Island, changed
866  synchronously, which suggests climate forcing (Miles et al., 2013). Law Dome is a promontory-
867  type ice rise with an independent flow center, and the saddle between this and the main ice sheet
868  is the source of the Totten and Vanderford Glaciers. A full-depth (1196-m long) ice core was
869  drilled near the summit of Law Dome and its high-resolution records have been used to determine
870  past climate changes (e.g., Van Ommen et al., 2004). The stable isotope record near the bed
871  indicates that Law Dome was not overridden by inland ice sheet during the LGM (Morgan et al.,
872  1997).  Geological evidence and GIA models suggest that Law Dome extended at least to the
873  middle of the continental shelf, and probably to near the shelf break, 40–65 km away from the
874  current ice margin, during the LGM and the adjacent ice sheet was a few hundred meters thicker
875  than present (Goodwin and Zweck, 2000). The ice-core-derived SMB during the LGM was about
876  one tenth of the present-day value, but this increased to the present-day value ~7 ka ago (Van
877  Ommen et al., 2004). Published radargrams over the summit vicinity (Hamley et al., 1986) do not
878  show Raymond arches, but the currently-available evidence is inadequate to confidently conclude
879  their absence.

880  The Sulzberger Ice Shelf (150° E), east of the Ross Sea, has numerous ice rises and
881  rumples (Fig. 3), but none have yet been studied. Upstream of this region (Marie Byrd Land)
882  there are numerous rock outcrops that have been used to constrain ice extent during the LGM and
883  the timing of Holocene deglaciation (Stone et al., 2003). Interpretations of such geological
884  records in a regional perspective are subject to how far these ice rises affect the upstream region.

885     Some ice rises and rumples exist in Coats Land (~30° W) between the Ronne-Filchner Ice
886  Shelf and DML. A much smaller ice-rise population in this region is distinct from the
887  neighboring DML, even though they have similar ice-shelf extents and proximities of the calving
888  front to the continental-shelf break. McDonald Ice Rumples (26° W) in the Brunt Ice Shelf were
889  first investigated by Limbert (1964) and Thomas (1971). They surveyed strain nets to determine
890  the effect of the ice rumples on the flow of the ice shelf (Section 3).

## 5.    Remaining challenges

892  Current understanding of ice rises and rumples is not sufficient to establish details of how they
893  contribute to the dynamics and evolution of the Antarctic Ice Sheet. Below we list (not
894  necessarily in order of importance) gaps in our understanding.

## 5.1 Net impact to ice-sheet and grounding-zone stability

896  Apart from the largest ice rises such as Roosevelt Island and Berkner Island, most ice rises and
897  rumples are smaller than the grid size of continent-scale ice-sheet models (Table 1). Thus, their
898  roles are only approximately evaluated in the context of continental or regional evolution.
899  Although a prognostic model with sophisticated mechanics has been used to study stability
900  effects (Favier et al., 2012), large-scale models using simpler mechanics (shallow-shelf
901  approximations) are unlikely to be able to resolve the horizontal shear around small nascent ice
902  rises. Further studies are needed to understand the consequences of the stabilizing effects of a
903  grounded feature for regional ice-sheet/shelf evolution.

904     To resolve the dynamical effects of small features, model-grid size matters (e.g., Durand
905  et al., 2009; Gladstone et al., 2012; Pattyn et al., 2012b). Studies using full-stress models with
906  sub-grid resolution (2.5 km x 50 m) have shown that small-scale ice rises and rumples exert
907  strong control on grounding-zone dynamics (e.g., Goldberg et al., 2009; Favier et al., 2012). To
908  overcome the problem of scale and fully evaluate buttressing effects, others have started to
909  include Schoof-type parameterizations of grounding-zone dynamics (Schoof, 2007; Schoof and
910  Hindmarsh, 2010) in large-scale models as a means to better replicate observations (Gladstone et
911  al., 2010; Pollard and DeConto, 2012). However, more observational data, including high-
912  resolution bathymetry (Section 5.4) and terrestrial geological records from inland sites, are
913  needed to further validate and develop both high-resolution numerical models and
914  parameterizations of the effects of small-scale pinning points on grounding-zone dynamics.

915     Even less researched are possible destabilizing effects from ice rises and rumples (Section
916  2.6.4). The formation of tensile zones around ice rises and rumples (Fig. 2) reduces the drag they
917  exert on the ice shelf. Moreover, weakening of shelves by crevassing likely increases calving,
918  reducing the extent of the shelf and potentially reducing buttressing effects (Hulbe et al., 2010;
919  Favier and Pattyn, 2015). Overall, it remains unclear whether the presence of ice rises can
920  destabilize an ice shelf and grounding zone, and if so, what is the combination of conditions (e.g.
921  location and distribution of ice rises, ice thickness, sea level) that might contribute to the
922  destabilization?

## 5.2 Interactions with ocean and sea ice

924  Ocean circulation and basal melting of ice shelves may influence the presence, position, and
925  shape of present-day ice rises, as well as their possible un-grounding in the future. The rapid
926  retreat of Thwaites and Pine Island Glaciers was initiated by un-grounding of the ice shelf from
927  an ice rumple near the grounding zone. Basal melting may have contributed to the un-grounding

928  of Thwaites (Jenkins et al., 2010a; Tinto and Bell, 2011). Similar un-grounding likely happens
929  elsewhere, but it remains unclear whether the presence of an ice rise or rumple would enhance or
930  reduce basal melt by itself. Possible high melt may also influence ocean circulation, in addition to
931  the effect of an elevated seabed around ice rises and rumples.

932  Coastal sea-ice distributions are affected by ice-shelf geometry and the presence of ice
933  rises near the calving front (e.g., Tamura et al., 2008). The wind field modified by these obstacles
934  often produces coastal polynyas to their west, and multi-year land-fast sea ice to their east (e.g.,
935  Massom et al., 2010). The former can increase sea-ice production, but such small changes are
936  difficult to detect using satellite data. Also, it remains unknown how a polynya's persistent
937  presence and proximity to an ice shelf affects the production of continental-shelf water and the
938  local ocean circulation and basal melting around nearby ice rises.

## 5.3 Equilibrium states and transitions between ice rises and rumples

939
940  We do not yet have sufficient knowledge of the geometries (e.g., ice draft, bathymetry) that allow
941  ice rises, rumples, or non-grounded ice to exist in an equilibrium state (i.e., phase diagrams). Nor
942  do we know details of how ice rises and rumples evolve. For example, what conditions can cause
943  an ice rumple to transition to an ice rise, and what conditions can cause the transition from an ice
944  rise to an ice rumple and/or to an ice shelf. Recent studies have suggested that ice rumples near
945  Bungenstock Ice Rise (Fig. 1) may be decaying (Brunt et al., 2011) or growing (Bradley et al.,
946  2015). Ongoing studies are needed to resolve these apparent inconsistencies.

947  Although the existence of many ice rises and rumples today suggests that they may be
948  relatively stable features, numerical-model evidence is inadequate to show their stability. An
949  elevated seabed is a necessary condition, but neither bed elevation nor ice thickness is sufficient
950  to distinguish between ice rises and rumples (Table 1, Fig. 4). Further, the apparent hysteresis
951  evident in the modeled evolution of ice rumples (Favier et al., 2012) suggests that non-linear
952  interactions are important.

## 5.4 Bed topography and geology

953
954  Bathymetry on the continental shelves, especially beneath the ice shelves, is not sufficient to
955  resolve small-scale seamounts that could be potential seeding sites for ice rises and rumples.
956  Similarly, potential locations of ice rises and rumples during glacial periods are not resolved,
957  which is consequential for the reconstruction of the expanded ice sheet during glacial periods. In
958  order to determine whether the ice grounded there, past water depths need to be accurately
959  modeled, and this necessitates the use of a coupled ice sheet-GIA model (Gomez et al., 2013; de
960  Boer et al., 2014).

961  Many ice rises and rumples exist close to each other (Fig. 1). Does this mean that the
962  conditions favorable to one are also favorable to the other, or does the presence of one produce
963  favorable conditions for the other? Bed topography and relative positions of ice rises and rumples
964  affect possible interactions within such clusters, which are difficult to investigate because of
965  poorly resolved bathymetry. Similarly, do disappearing ice rises result in multiple, smaller
966  grounded features that interact with each other and cause as-yet-undocumented complications?
967  For example, many promontory-type ice rises have a local ice dome on the seaward side and a
968  saddle towards the ice sheet. An ice rise at 24° E in DML has an elevated bed under the ice dome
969  and a lowered bed under the saddle (Matsuoka et al., 2012; K. Matsuoka and F. Pattyn,
970  unpublished data). When deglaciation occurs, this feature may separate into an isle-type ice rise

971 seaward of a smaller promontory-type ice rise (Favier and Pattyn, 2015). A pair of such (possibly
972 separated) ice rises is located at 16° E in DML.

973 The evolution of ice rises has been examined using radar-detected englacial stratigraphy
974 and ice-flow models. For such modeling, radar-measured bed topography is available only
975 beneath the grounded ice. Realistic bathymetry around the grounded ice is also needed to
976 adequately model the grounding-zone position. Similarly, prognostic modeling of ice rises
977 requires knowledge of the bed topography over the expanded extent of the ice rise. To determine
978 bathymetry that can delineate seeding sites for ice rises and possible grounding-zone positions,
979 vibroseismic measurements under ice shelves (Eisen et al., 2014) and multi-beam sonar
980 soundings are necessary. Geological knowledge is also obtainable with these methods, and it is
981 needed to evaluate basal stresses of the grounded features, especially when the ice-bed interface
982 is nearly thawed, which likely happens during the initial and terminal stages of an ice rise. It can
983 also shed light on the seabed geology in areas that are otherwise more difficult to reach.

## 984 5.5 Ice core science: paleo-climate and chronology for ice-rise
## 985 evolution

986 Stable ice rises are ideal sites to drill ice cores. The large SMB permits the retrieval of high-
987 resolution temporal records over the past millennia. The International Partnership of Ice Core
988 Science (IPICS) proposed ice cores that cover the past 2 ka and the entire LGM-Holocene
989 transition and beyond (40-ka initiative). The relatively short characteristic times (Fig. 10) limit
990 the range of the period covered by an ice-rise core, but most large ice rises are potential sites for
991 the IPICS 2-ka initiative, and several are suitable for the IPICS 40-ka initiative (Mulvaney et al.,
992 2007; Bertler et al., 2014; Mulvaney et al., 2014). Dense arrays of high temporal-resolution cores
993 are needed to examine the spatial and temporal variability of atmospheric dynamics such as the
994 El Nino-Southern Oscillation (e.g., Naik et al., 2010). The proximity of ice rises to the ocean
995 makes them sensitive to regional climate and ocean variability.

996 Ice cores can help constrain the evolution of ice rises. For example, air trapped in bubbles
997 in the ice can reveal histories of surface elevations and whether the ice rise is long-term emergent
998 over a glacial-interglacial cycle. In addition, age-depth profiles from ice cores can be used to date
999 radar-detected stratigraphy, which helps constrain the histories of climate and ice dynamics
1000 (Waddington et al., 2005).

## 1001 5.6 Integrated science of inter-connected elements in Antarctica

1002 Understanding the past, present and future of the Antarctic Ice Sheet requires a complete
1003 description of both the interior and coastal systems. The coastal system involves non-linear
1004 interactions between ice, ocean and the atmosphere. Although understanding of these interactions
1005 is improving, challenges still remain. A major challenge is that, although ice rises and rumples
1006 are small, their contributions to grounding-zone stability (instability) can be large. Because
1007 ephemerally-grounded features provide little buttressing (Schmeltz et al., 2001), evolution of ice
1008 rises and rumples may have threshold-like impacts on ice-sheet dynamics as the shelf ice grounds
1009 and un-grounds. Uneven distribution of ice rises and rumples around Antarctica lead to different
1010 regional characteristics. We do not know how much individual Antarctic regions contributed to
1011 rapid pulses of sea-level rise, such as MWP1a (Bentley et al., 2010; 2014; Weber et al., 2014).
1012 Exploring ice rises is a viable way to address the Holocene behavior of the ice sheet at a high
1013 temporal resolution. To decipher the evolution of the Antarctic Ice Sheet, we first need to
1014 describe the system science in the coastal region.

## Acknowledgements

This manuscript is an outcome of an International Workshop on Antarctic Ice Rises held at the Norwegian Polar Institute (NPI) in Tromsø, 2013. We acknowledge sponsors of this workshop: Standing Science Group on Physical Sciences of the Scientific Committee on Antarctic Research (SCAR), World Climate Research Programme's Climate and Cryosphere (CliC) project, Association of Polar Early Career Scientists (APECS), Research Council of Norway's MILUTV-ARENAER program, British Antarctic Survey, and NPI's Center for Ice, Climate, and Ecosystems. Figure 2 was constructed by Audun Igesund of NPI and Figure 7 by Chris Orton of Durham University. Maps in this paper (Figs. 1, 3, 5, 6, 10) were prepared using Quantarctica (www.quantarctica.org). Workshop outcomes, such as talk slides and video, posters, and short video clips (FrostBytes) introducing poster presentations for non specialists are hosted by CliC and available at http://www.climate-cryosphere.org/meetings/past/2013/ice-rises-2013.

## Appendix: Inventory of ice rises and rumples

The inventory is based on available grounding-zone products and some additional visual interpretation of satellite imagery. Beginning with the island polygons of the MODIS Mosaic of Antarctica (MOA) 2003-2004 product (Haran et al., 2005; Scambos et al., 2007), we extracted all island polygons that were contained within an ice shelf, assuming that they represent ice rises or rumples. We then updated this dataset using the new MOA 2009 product as well as independent grounding-zone points from SAR interferometry (Rignot et al., 2011) and ICESat altimetry (Fricker et al., 2009; Brunt et al., 2010). This preliminary inventory was then manually edited and updated based on visual interpretation of the two MOA image mosaics, the high-resolution Landsat Image Mosaic of Antarctica (LIMA) (Bindschadler et al., 2008), and the IPY-MEaSUREs Antarctica velocity map (Rignot et al., 2011). We also digitized polygons around the most prominent ice ridges and domes within the continental grounding zone.

The grounded features fall into four groups. The first group is identified by clearly elevated features that are very likely isle-type ice rises surrounded by ice shelves and is labeled 'identifier 1' in the inventory and Table 1. The second group is identified by prominent ice ridges and domes connected to the inland ice sheet (promontory-type ice rises, 'identifier 2'). Their landward extent is often hard to discern. We do not use a clear criterion to include or not such features in this inventory; the inventoried features are samples that either have been investigated or could be interesting research targets. The third group is identified by less-prominent grounded isles that show more diffuse, dynamic characteristics. Such features include ice rumples ('identifier 3'). The fourth group is similar to the first group but features have outcropping bedrock or sediments (Scientific Committee on Antarctic Research, 2012) within the grounded features ('identifier 4').

Attributes of individual features are provided in the inventory and associated population statistics are presented in Table 1 and Fig. 4, which are discussed in Section 2.4. These attributes include: maximum, minimum and mean values of bed elevations and ice-surface elevations, maximum ice thickness, mean ice-surface slope, relative height of the highest place (summit) of the feature measured from the adjacent ice shelf or stream surface (all data are from the Bedmap2 dataset (Fretwell et al., 2013)), and mean ice-flow speed (Rignot et al., 2011). These datasets have grid sizes of 1 km, so may include large errors associated with the spatial extent of the grounded features. Elevations are referenced to the GL04C geoid, which is used for the Bedmap2 dataset (Fretwell et al., 2013).

1059   This inventory is aimed to provide an approximate picture of their continent-wide
1060   distribution and overall characteristics; there are likely many undetected features. The inventory
1061   is    provided    through    a    data    center    at    the    Norwegian    Polar    Institute:
1062   data.npolar.no/dataset/9174e644-3540-44e8-b00b-c629acbf1339. We provide this inventory in a
1063   shape file format with an associated GIS style file that enable use of the inventory as part of free-
1064   GIS data package "Quantarctica" downloadable at www.quantarctica.org.

1065

1066 # Tables

1067 **Table 1**. Types and characteristics of ice rises and rumples. For rows of area and below, the first
1068 number in each cell shows the median value, and two numbers in parentheses indicate the first
1069 and third quarter values.

| | Ice rises (isles) | Ice rises (promontory)[*1] | Ice rumples | Elevated features with outcrops |
|---|---|---|---|---|
| Identifier in the inventory | 1 | 2 | 3 | 4 |
| Number | 103 | 67 | 510 | 24 |
| Total area (km$^2$) | $1.18 \times 10^5$ | $2.07 \times 10^5$ | $8.52 \times 10^3$ | $1.88 \times 10^3$ |
| Area (km$^2$) | 151 (30, 560) | 951 (398, 3202) | 3.2 (1.2, 8.5) | 16.0 (5.3, 91.2) |
| Longest axis length (km)[*2] | 13.9 (6.7, 26.0) | 35.9 (24.7, 63.7) | 1.2 (0.4, 3.2) | 3.4 (1.4, 12.2) |
| orthogonal axis length (km)[*2] | 3.0 (0, 6.1) | 5.1 (0, 12.3) | 0 (0, 0) | 0.98 (0, 1.6) |
| Aspect ratio | 0.17 (0, 0.28) | 0.18 (0, 0.33) | 0 (0, 0) | 0.26 (0, 0.34) |
| Maximum height (m)[*3] | 168 (56, 361) | 553 (400, 659) | 51 (36, 70) | 55 (25, 128) |
| Maximum relative height from the adjacent ice (m)[*3] | 120 (13, 306) | 501 (334, 608) | 2 (1, 6) | 16 (8, 80) |
| Mean slope (degrees)[*3] | 0.69 (0.14, 1.35) | 1.26 (0.97, 1.66) | 0.11 (0.07, 0.16) | 0.27 (0.12, 0.97) |
| Maximum ice thickness (m)[*3] | 292 (219, 375) | 433 (357, 643) | 372 (253, 527) | 58 (31, 137) |
| Mean bed elevation (m)[*3] | -186 (-267, -119) | -178 (-311, -119) | -323 (-460, -221) | -19 (-67, -5) |
| Range of the bed-elevation variations (m)[*3] | 233 (99, 421) | 564 (453, 714) | 15 (4, 39) | 140 (58, 398) |
| Maximum flow speed (m/a)[*3] | 13 (6, 23) | 14 (7, 22) | 67 (29, 144) | 7 (5, 11) |

1070 *1: Sometimes called ice ridges or domes, a continuous feature of the continental ice sheet.
1071 Inland boundaries of these features are poorly defined, so spatial extent and relevant parameters
1072 are inaccurate.

1073 *2: The orthogonal axis is defined relative to the longest axis.

1074 *3: Surface elevation, bed elevation, and ice thickness data are from Fretwell et al. (2013). Ice-
1075 flow speed data are from Rignot et al. (2011) . Grid size of these datasets is ~1 km, so large errors
1076 may be associated with the spatial extent and other properties of the grounded features.
1077 Elevations are referenced to the GL04C geoid, which is used for the Bedmap2 dataset (Fretwell
1078 et al., 2013).

1079 **<u>Figures</u>**
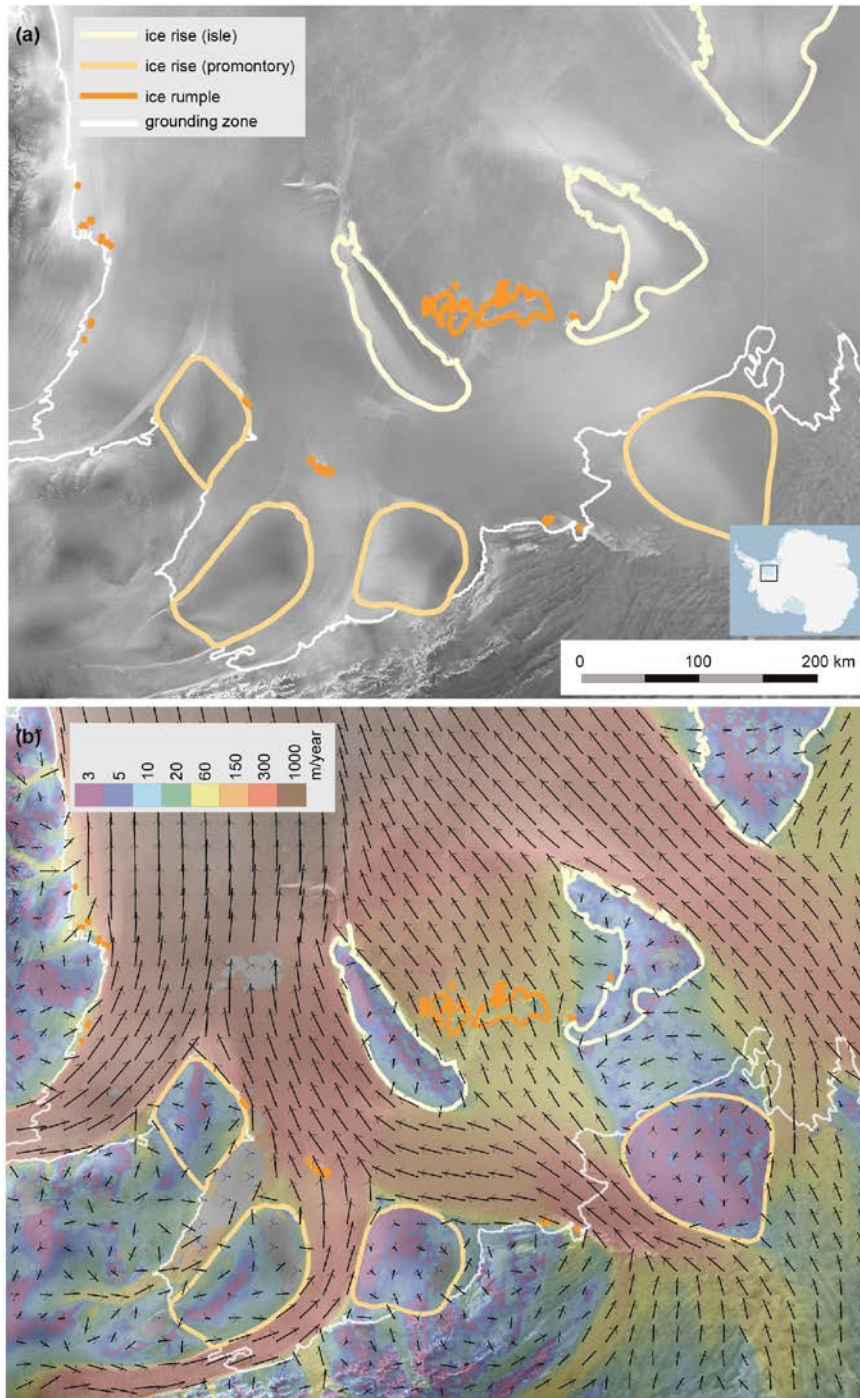


1080
1081 **Figure 1 (2 columns)**: Ice rises and rumples in the Ronne-Filchner Ice Shelf, West Antarctica.
1082 Inset shows the location. Outlined are ice rises and rumples inventoried in this study (see
1083 Appendix). Bed topography in this region and names of these ice rises and rumples are shown in
1084 Figure 6b. The grounding zone of the ice sheet is also shown (Bindschadler et al., 2011). (a)
1085 Morphological structures associated with ice rises and rumples visible in Radarsat-2 satellite
1086 imagery (Jezek et al., 2002). Brightness changes are associated with surface-slope variations of
1087 major ice rises, as well as crevasses and rifts in the ice shelf. (b) Ice flow field (Rignot et al.,

1088  2011) perturbed by ice rises and rumples. Arrow lengths are proportional to the logarithm of ice-
1089  flow speeds.
1090
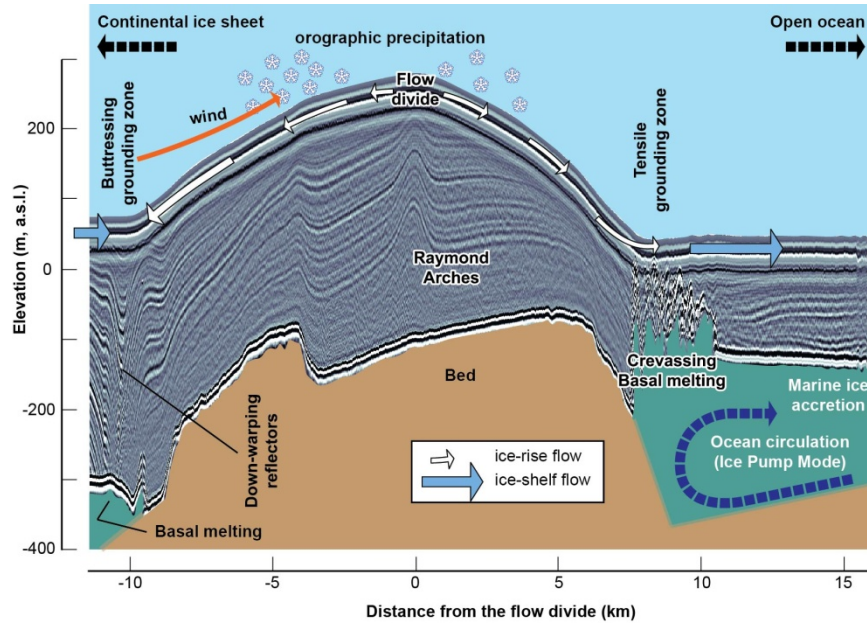


1091
1092
1093  **Figure 2 (2 columns)**: Cross section of an ice rise. The radargram is from an along-flow, ground-
1094  based profile across the summit of Kupol Ciolkovskogo near the Fimbul Ice Shelf, Dronning
1095  Maud Land (K. Matsuoka and J. Brown, unpublished data). Dominant wind direction is oblique
1096  to the cross section, and seabed beneath the ocean cannot be detected using radar. The sketches of
1097  orographic precipitation and seabed are included for illustration purposes.
1098
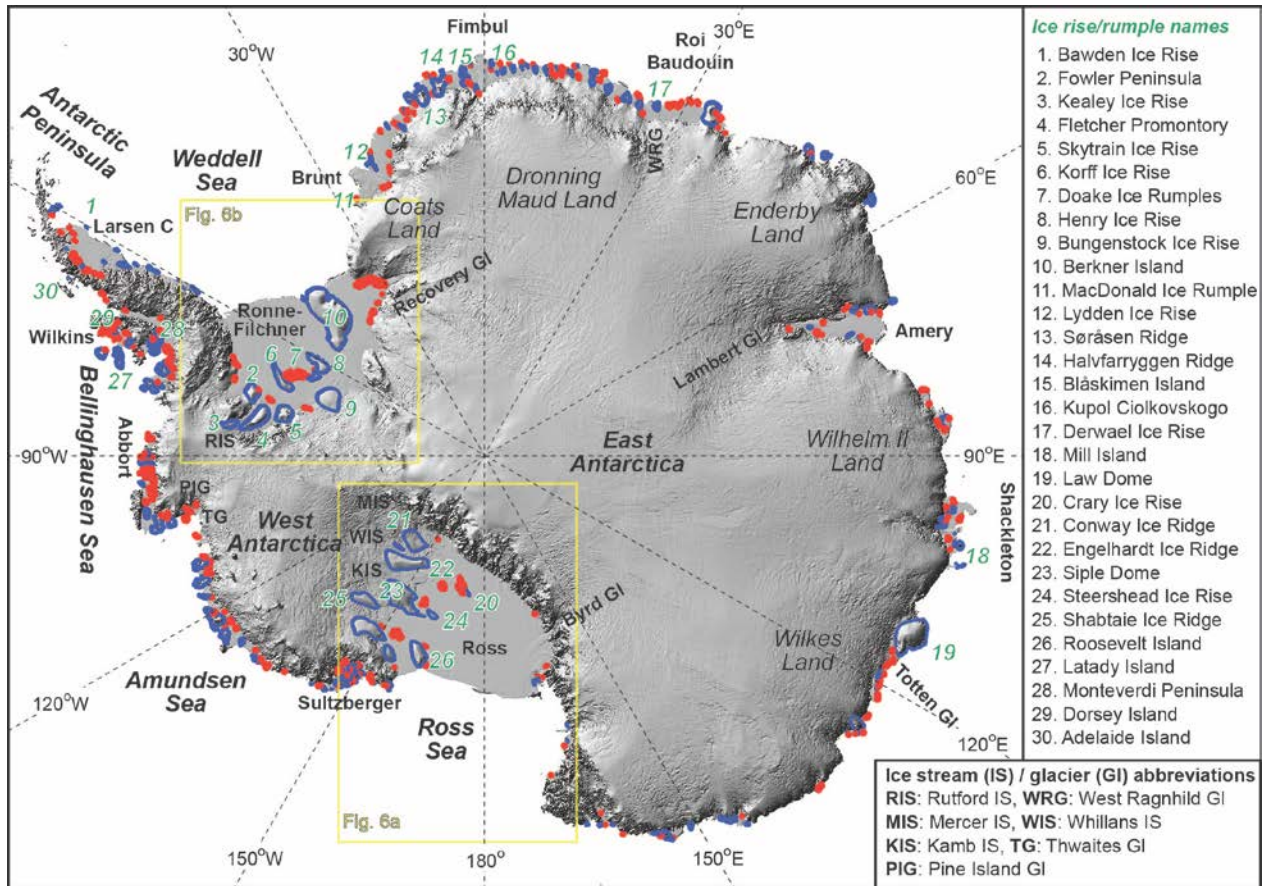
**Figure 3 (two columns)**: Locations of ice rises (blue, outlined) and ice rumples (red) in Antarctica, which are included in the inventory (Appendix). Red markers for ice rumples do not represent their dimensions. The background image is a shaded relief map of the Bedmap2 digital elevation model (Fretwell et al., 2013). Ice streams, glaciers, and ice shelves mentioned in the text are labeled and major ice rises and rumples are indicated with numbers. Bed topography in the Ross and Weddell Seas are shown in Figs. 6a and 6b, respectively.

1107
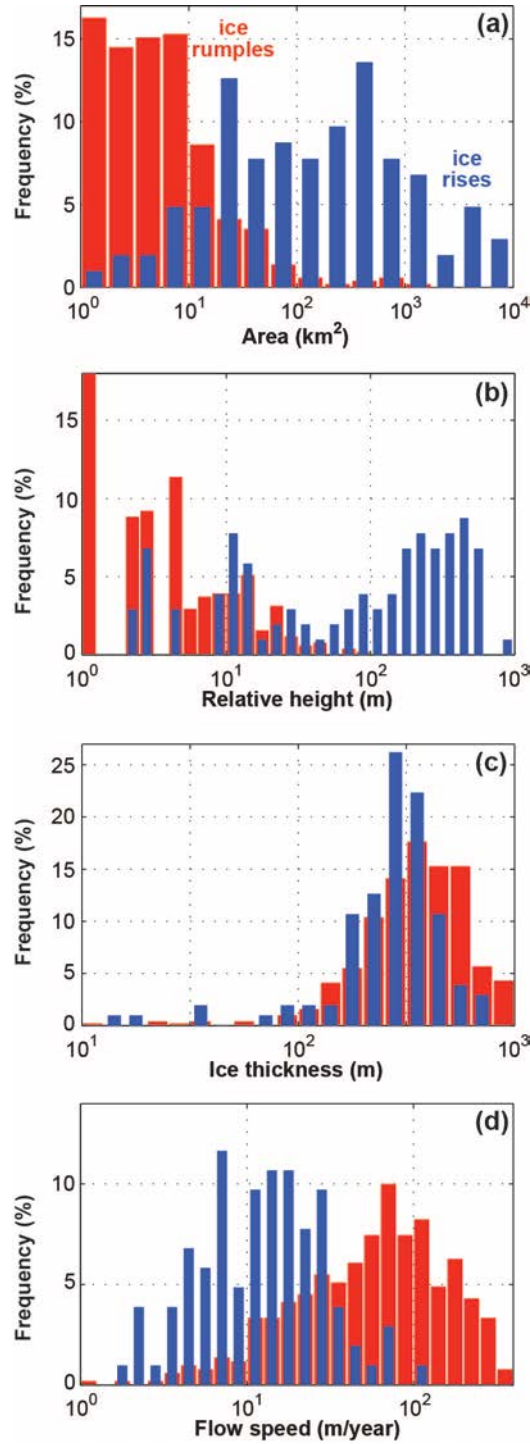
**Figure 4 (one column)**: Population characteristics of ice rises and rumples. Panels show histograms of (a) area, (b) relative height of the highest place (summit) of ice rises/rumples measured from the adjacent ice shelf/stream surface, (c) maximum ice thickness, and (d) maximum flow speeds within the ice rises and rumples. All abscissas have a logarithm scale, and frequency is shown in percent of a total of the 103 isle-type ice rises and 510 ice rumples inventoried in this study (Table 1).
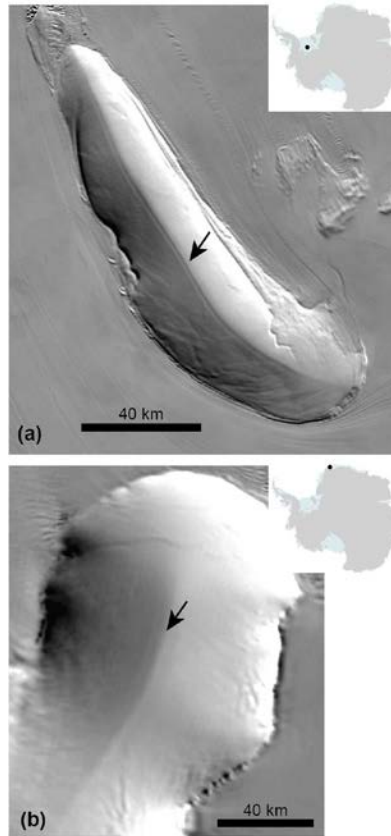
1114

**Figure 5 (one column)**: Near-parallel lineations (shown with arrows) along the ice-flow divide detected by MODIS satellite imagery (Haran et al., 2005; Scambos et al., 2007). Other lineations in the flank are often associated with the slope changes. (a) Korff Ice Rise in the Weddell Sea (Smith, 1986), which has a (single-peaked) Raymond arches (J. Kingslake, unpublished data). (b) Halvfarryggen Ridge in Dronning Maud Land, which has double-peaked Raymond arches (Drews et al., 2013). For Raymond arches, see Section 4.1.
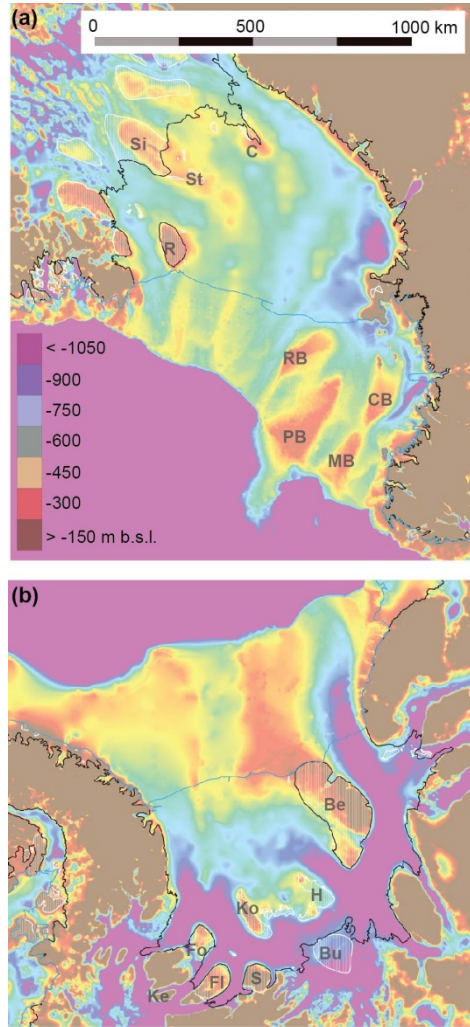
1121

**Figure 6 (one column)**: Elevated bed topography beneath ice rises and rumples in the Ross (a) and Weddell (b) Sea Embayments. Bed elevations are referenced to the GL04C geoid (Fretwell et al., 2013); geoid heights are ~40 m in the Ross Sea and ~20 m in the Weddell Sea. Outlined are the grounding zone (black; Bindschadler et al., 2011) and current ice-shelf's calving front (blue; Scientific Committee on Antarctic Reseach, 2012). Inventoried ice rises and rumples (Appendix) are hatched, and labels are given to major ice rises. In Panel (a), labeled are Siple Dome (Si), Roosevelt Island (R), Crary Ice Rise (C), and Steershead Ice Rise (St), as well as likely locations of ice rises during the LGM (Shipp et al., 1999): Crary Bank (CB), Mawson Bank (MB), Pennell Bank (PB) and Ross Bank (RB). In panel (b), labeled are the current ice rises and rumples: Berkner Island (Be), Henry Ice Rise (H), Korff Ice Rise (K), Bungenstock Ice Rise (Bu), Skytrain Ice Rise (S), Kealey Ice Rise (Ke), Fletcher Promontory (Fl), and Fowler Peninsula (Fo).
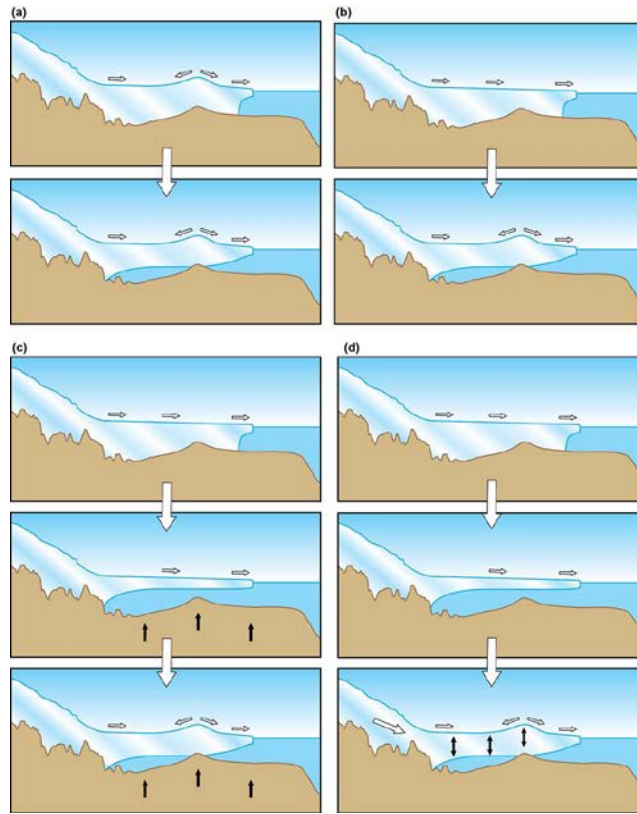
1133

**Figure 7 (1.5 column)**: Possible formation mechanisms for isle-type ice rises. (a) Long-term stable. (b) Deglacial emergent. (c) GIA emergent. (d) Glaciological emergent. For each case, the evolution is shown in scenes connected by large open downward arrows between panels. Open arrows within individual panels illustrate the direction of ice flow, whereas solid black arrows illustrate the emerging bed associated with GIA (c) and a thickening ice shelf (d). Corresponding changes of ice elevation are shown in Fig. 8.

1140
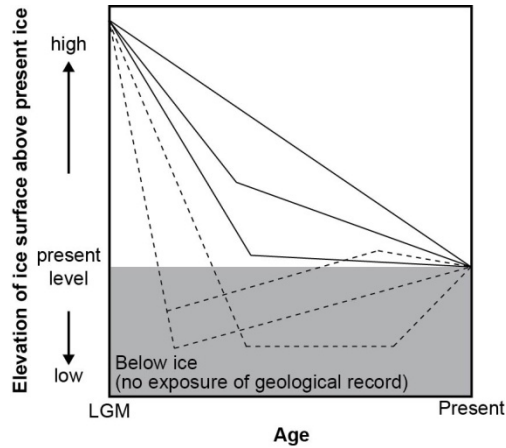
1141

**Figure 8 (one column)**: Surface-elevation changes of the ice sheet upstream of ice rises, associated with the ice-rise formation mechanisms shown in Fig. 7. Solid lines show cases of long-term stable and deglacial emergent (Figs. 7a and 7b). Dashed lines show GIA and glaciological emergent (Figs. 7c and 7d). Elevation changes in the shaded area occur below the current ice surface so geological records are not exposed.

1147
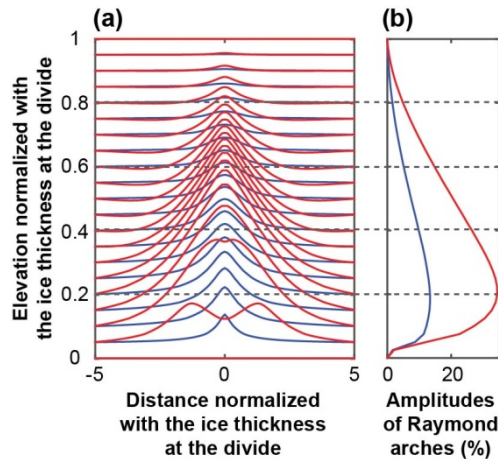


1148

**Figure 9 (one column)**: Properties of Raymond arches. (a) Cross section of modeled isochrones. (b) Depth variations of the arch amplitudes relative to the ice thickness at the divide. In both panels, blue shows a case of isotropic ice resulting in single-peak Raymond arches, and red shows a case of anisotropic ice induced by development of ice-crystal alignments resulting in double-peaked arches. The figure shows steady-state model results presented in Fig. 11b of Martin et al. (2009a).

1155

1156
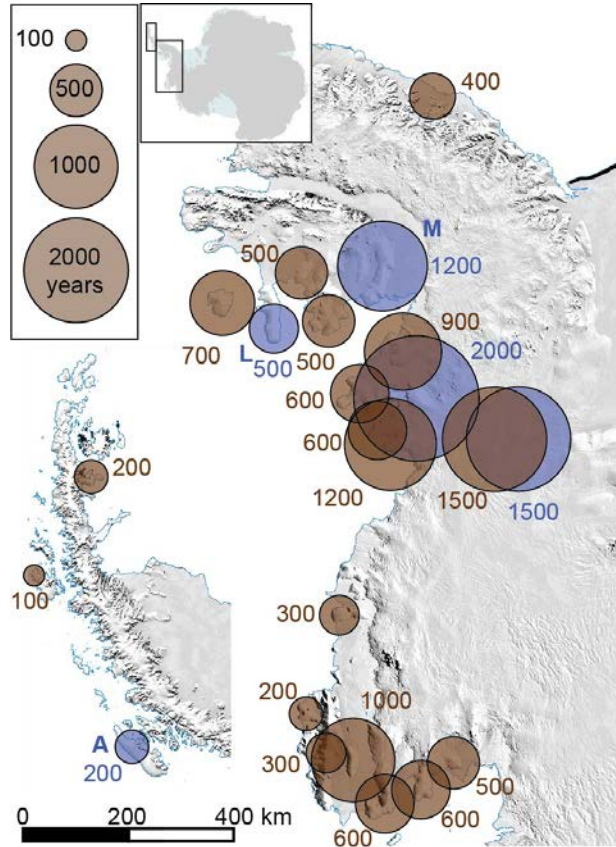
1157

**Figure 10 (one column)**: Twenty three ice rises in the Antarctic Peninsula and Amundsen Sea coast that show a pair of distinct near-parallel lineations in satellite imagery in the central part of the ice rise (similar to those shown in Fig. 5). Inset shows the location. Numbers are the characteristic ice-flow time scale $T$ ($= H/b$ in years, where $H$ is ice thickness and $b$ is SMB). The five ice rises shown with blue circles have well-developed, double-peaked Raymond arches (Fig. 9a); Adelaide Island (labeled as A), Latady Island (L) and Monteverdi Peninsula (M) were surveyed with ground-based radar and the other two with airborne radar. Background satellite image is Landsat (Bindschadler et al., 2008), and the calving front is highlighted in blue (Scientific Committee on Antarctic Research, 2012).

1167

## References

1169 Anderson, J.B., 1999. Antarctic marine geology. Cambridge University Press, Cambridge.

1170 Anderson, J.B., Conway, H., Bart, P.J., Witus, A.E., Greenwood, S.L., McKay, R.M., Hall, B.L.,
1171     Ackert, R.P., Licht, K., Jakobsson, M. and Stone, J.O., 2014. Ross Sea paleo-ice sheet
1172     drainage and deglacial history during and since the LGM. Quaternary Science Reviews,
1173     100: 31-54.

1174 Arndt, J.E., Schenke, H.W., Jakobsson, M., Nitsche, F.O., Buys, G., Goleby, B., Rebesco, M.,
1175     Bohoyo, F., Hong, J., Black, J., Greku, R., Udintsev, G., Barrios, F., Reynoso-Peralta, W.,
1176     Taisei, M. and Wigley, R., 2013. The International Bathymetric Chart of the Southern
1177     Ocean (IBCSO) Version 1.0 – A new bathymetric compilation covering circum-Antarctic
1178     waters. Geophysical Research Letters, 40: 3111-3117.

1179 Arthern, R.J., Winebrenner, D.P. and Vaughan, D.G., 2006. Antarctic snow accumulation
1180     mapped using polarization of 4.3-cm wavelength microwave emission. Journal of
1181     Geophysical Research-Atmospheres, 111(D6): D06107.

1182 Årthun, M., Nicholls, K.W., Makinson, K., Fedak, M.A. and Boehme, L., 2012. Seasonal inflow
1183     of warm water onto the southern Weddell Sea continental shelf, Antarctica. Geophysical
1184     Research Letters, 39(17): L17601.

1185 Årthun, M., Nicholls, K.W. and Boehme, L., 2013. Wintertime Water Mass Modification near an
1186     Antarctic Ice Front. Journal of Physical Oceanography, 43(2): 359-365.

1187 Balco, G. and Schaefer, J.M., 2013. Exposure-age record of Holocene ice sheet and ice shelf
1188     change in the northeast Antarctic Peninsula. Quaternary Science Reviews, 59: 101-111.

1189 Bamber, J.L., Gomez-Dans, J.L. and Griggs, J.A., 2009. A new 1 km digital elevation model of
1190     the Antarctic derived from combined satellite radar and laser data ‚Äì Part 1: Data and
1191     methods. The Cryosphere, 3(1): 101-111.

1192 Bentley, M.J., Fogwill, C.J., Le Brocq, A.M., Hubbard, A.L., Sugden, D.E., Dunai, T.J. and
1193     Freeman, S.P.H.T., 2010. Deglacial history of the West Antarctic Ice Sheet in the
1194     Weddell Sea embayment: Constraints on past ice volume change. Geology, 38(5): 411-
1195     414.

1196 Bentley, M.J., Cofaigh, C.O., Anderson, J.B., Conway, H., Davies, B., Graham, A.G.C.,
1197     Hillenbrand, C.-D., Hodgson, D.A., Jamieson, S.S.R., Larter, R.D., Mackintosh, A.,
1198     Smith, J.A., Verleyen, E., Ackert, R.P., Bart, P.J., Berg, S., Brunstein, D., Canals, M.,
1199     Colhoun, E.A., Crosta, X., Dickens, W.A., Domack, E., Dowdeswell, J.A., Dunbar, R.,
1200     Ehrmann, W., Evans, J., Favier, V., Fink, D., Fogwill, C.J., Glasser, N.F., Gohl, K.,
1201     Golledge, N.R., Goodwin, I., Gore, D.B., Greenwood, S.L., Hall, B.L., Hall, K., Hedding,
1202     D.W., Hein, A.S., Hocking, E.P., Jakobsson, M., Johnson, J.S., Jomelli, V., Jones, R.S.,
1203     Klages, J.P., Kristoffersen, Y., Kuhn, G., Leventer, A., Licht, K., Lilly, K., Lindow, J.,
1204     Livingstone, S.J., Masse, G., McGlone, M.S., McKay, R.M., Melles, M., Miura, H.,
1205     Mulvaney, R., Nel, W., Nitsche, F.O., O'Brien, P.E., Post, A.L., Roberts, S.J., Saunders,
1206     K.M., Selkirk, P.M., Simms, A.R., Spiegel, C., Stolldorf, T.D., Sugden, D.E., van der
1207     Putten, N., van Ommen, T., Verfaillie, D., Vyverman, W., Wagner, B., White, D.A.,
1208     Witus, A.E., Zwartz, D. and Consortium, R., 2014. A community-based geological
1209     reconstruction of Antarctic Ice Sheet deglaciation since the Last Glacial Maximum.
1210     Quaternary Science Reviews, 100: 1-9.

1211 Bertler, N., Conway, H., Dahl-Jensen, D., Blunier, T., Brook, E., Dadic, R., Delmonte, B.,
1212     Dongqi, Z., Edwards, R., Emanuelsson, D., Fudge, T., Golledge, N., Hindmarsh, R.,
1213     Hawley, R., Kipfstuhl, S., Kjaer, H., Kurbatov, A., Lee, J., Mayewski, P.A., Naish, T.,

Neff, P., Scherer, R., Severinghaus, J., Simonsen, M., Steig, E.J., Tuohy, A., Vallenlonga, P. and Waddington, E.D., 2014. The Roosevelt Island Climate Evolution (RICE) Project – Did the Ross Ice Shelf Collapse During MIS 5e?, AGU fall meeting. AGU, San Francisco.

Bindschadler, R., Roberts, E.P. and Iken, A., 1990. Age of Crary Ice Rise, Antarctica, determined from temperature-depth profiles. Annals of Glaciology, 14(1): 13-16.

Bindschadler, R., 1993. Siple Coast project research of Crary Ice Rise and the months of Ice Stream B and Ice Stream C, West Antarctica - review and new perspectives. Journal of Glaciology, 39(133): 538-552.

Bindschadler, R., Vornberger, P., Fleming, A., Fox, A., Mullins, J., Binnie, D., Paulsen, S.J., Granneman, B. and Gorodetzky, D., 2008. The Landsat Image Mosaic of Antarctica. Remote Sensing of Environment, 112(12): 4214-4226.

Bindschadler, R., Choi, H., Wichlacz, A., Bingham, R., Bohlander, J., Brunt, K., Corr, H., Drews, R., Fricker, H., Hall, M., Hindmarsh, R., Kohler, J., Padman, L., Rack, W., Rotschky, G., Urbini, S., Vornberger, P. and Young, N., 2011. Getting around Antarctica: new high-resolution mappings of the grounded and freely-floating boundaries of the Antarctic ice sheet created for the International Polar Year. Cryosphere, 5(3): 569-588.

Bindschadler, R.A., Roberts, E.P. and Macayeal, D.R., 1989. Distribution of net mass balance in the vicinity of Crary Ice Rise, Antarctica. Journal of Glaciology, 35(121): 370-377.

Blindow, N., Suckro, S.K., Rueckamp, M., Braun, M., Schindler, M., Breuer, B., Saurer, H., Simoes, J.C. and Lange, M.A., 2010. Geometry and thermal regime of the King George Island ice cap, Antarctica, from GPR and GPS. Annals of Glaciology, 51(55): 103-109.

Borstad, C.P., Rignot, E., Mouginot, J. and Schodlok, M.P., 2013. Creep deformation and buttressing capacity of damaged ice shelves: theory and application to Larsen C ice shelf. Cryosphere, 7(6): 1931-1947.

Bradley, S.L., Hindmarsh, R.C.A., Whitehouse, P.L., Bentley, M.J. and King, M.A., 2015. Low post-glacial rebound rates in the Weddell Sea due to Late Holocene ice-sheet readvance. Earth and Planetary Science Letters, 413: 79-89.

Braun, M., Humbert, A. and Moll, A., 2009. Changes of Wilkins Ice Shelf over the past 15 years and inferences on its stability. Cryosphere, 3(1): 41-56.

Brook, E.J., White, J.W.C., Schilla, A.S.M., Bender, M.L., Barnett, B., Severinghaus, J.P., Taylor, K.C., Alley, R.B. and Steig, E.J., 2005. Timing of millennial-scale climate change at Siple Dome, West Antarctica, during the last glacial period. Quaternary Science Reviews, 24(12-13): 1333-1343.

Brunt, K.M., Fricker, H.A., Padman, L., Scambos, T.A. and O'Neel, S., 2010. Mapping the grounding zone of the Ross Ice Shelf, Antarctica, using ICESat laser altimetry. Annals of Glaciology, 51(55): 71-79.

Brunt, K.M., Fricker, H.A. and Padman, L., 2011. Analysis of ice plains of the Filchner-Ronne Ice Shelf, Antarctica, using ICESat laser altimetry. Journal of Glaciology, 57(205): 965-975.

Callens, D., Matsuoka, K., Steinhage, D., Smith, B., Witrant, E. and Pattyn, F., 2014. Transition of flow regime along a marine-terminating outlet glacier in East Antarctica. Cryosphere, 8(3): 867-875.

Catania, G., Hulbe, C. and Conway, H., 2010. Grounding-line basal melt rates determined using radar-derived internal stratigraphy. Journal of Glaciology, 56(197): 545-554.

1259 Catania, G., Hulbe, C., Conway, H., Scambos, T.A. and Raymond, C.F., 2012. Variability in the
1260         mass flux of the Ross ice streams, West Antarctica, over the last millennium. Journal of
1261         Glaciology, 58(210): 741-752.
1262 Chavanne, C.P., Heywood, K.J., Nicholls, K.W. and Fer, I., 2010. Observations of the Antarctic
1263         Slope Undercurrent in the southeastern Weddell Sea. Geophysical Research Letters, 37:
1264         L13601.
1265 Conway, H., Hall, B.L., Denton, G.H., Gades, A.M. and Waddington, E.D., 1999. Past and future
1266         grounding-line retreat of the West Antarctic Ice Sheet. Science, 286(5438): 280-283.
1267 Conway, H., Catania, G., Conway, M., Rasmussen, L.A., Raymond, C.F., Marshall, H.P. and
1268         O'Neel, S., 2005. Glacial history of the ridge between Mercer and van der Veen Ice
1269         Streams, 12th Annual WAIS Workshop, Sterling, VA.
1270 Cook, A.J. and Vaughan, D.G., 2010. Overview of areal changes of the ice shelves on the
1271         Antarctic Peninsula over the past 50 years. The Cryosphere, 4(1): 77-98.
1272 Craven, M., Allison, I., Fricker, H.A. and Warner, R., 2009. Properties of a marine ice layer
1273         under the Amery Ice Shelf, East Antarctica. Journal of Glaciology, 55(192): 717-728.
1274 Cuffey, K.M. and Paterson, W.S.B., 2010. The Physics of Glaciers.
1275 de Boer, B., Stocchi, P. and van de Wal, R.S.W., 2014. A fully coupled 3-D ice-sheet-sea-level
1276         model: algorithm and applications. Geoscientific Model Development, 7(5): 2141-2156.
1277 De Rydt, J., Holland, P.R., Dutrieux, P. and Jenkins, A., 2014. Geometric and oceanographic
1278         controls on melting beneath Pine Island Glacier. Journal of Geophysical Research-
1279         Oceans, 119(4): 2420-2438.
1280 Depoorter, M.A., Bamber, J.L., Griggs, J.A., Lenaerts, J.T.M., Ligtenberg, S.R.M., van den
1281         Broeke, M.R. and Moholdt, G., 2013. Calving fluxes and basal melt rates of Antarctic ice
1282         shelves. Nature, 502(7469): 89-93.
1283 Dinniman, M.S., Klinck, J.M. and Hofmann, E.E., 2012. Sensitivity of Circumpolar Deep Water
1284         Transport and Ice Shelf Basal Melt along the West Antarctic Peninsula to Changes in the
1285         Winds. Journal of Climate, 25(14): 4799-4816.
1286 Doake, C.S.M., Corr, H.F.J., Rott, H., Skvarca, P. and Young, N.W., 1998. Breakup and
1287         conditions for stability of the northern Larsen Ice Shelf, Antarctica. Nature, 391(6669):
1288         778-780.
1289 Drews, R., Martín, C., Steinhage, D. and Eisen, O., 2013. Characterizing the glaciological
1290         conditions at Halvfarryggen ice dome, Dronning Maud Land, Antarctica. Journal of
1291         Glaciology, 59(213): 9-20.
1292 Drews, R., Matsuoka, K., Martín, C., Callens, D., Bergeot, N. and Pattyn, F., 2015. Evolution of
1293         Derwael Ice Rise in Dronning Maud Land, Antarctica, over the last millennia. Journal of
1294         Geophysical Research: Earth Surface, 120: 2014JF003246.
1295 Durand, G., Gagliardini, O., de Fleurian, B., Zwinger, T. and Le Meur, E., 2009. Marine ice sheet
1296         dynamics: Hysteresis and neutral equilibrium. Journal of Geophysical Research-Earth
1297         Surface, 114: F03009.
1298 Eisen, O., Hofstede, C., Diez, A., Kristoffersen, Y., Lambrecht, A., Mayer, C., Blenkner, R. and
1299         Hilmarsson, S., 2014. On-ice vibroseis and snowstreamer systems for geoscientific
1300         research. Polar Science, 9(1): 51-65.
1301 Fahnestock, M.A., Scambos, T.A., Bindschadler, R.A. and Kvaran, G., 2000. A millennium of
1302         variable ice flow recorded by the Ross Ice Shelf, Antarctica. Journal of Glaciology,
1303         46(155): 652-664.
1304 Farrell, W.E. and Clark, J.A., 1976. On Postglacial Sea Level. Geophysical Journal of the Royal
1305         Astronomical Society, 46(3): 647-667.

1306     Favier, L., Gagliardini, O., Durand, G. and Zwinger, T., 2012. A three-dimensional full Stokes
1307         model of the grounding line dynamics: effect of a pinning point beneath the ice shelf.
1308         Cryosphere, 6(1): 101-112.
1309     Favier, L. and Pattyn, F., 2015. Antarctic ice-rise formation, evolution and stability. Geophys.
1310         Res. Lett., 42(11): 4456-4463.
1311     Fernandoy, F., Meyer, H., Oerter, H., Wilhelms, F., Graf, W. and Schwander, J., 2010. Temporal
1312         and spatial variation of stable-isotope ratios and accumulation rates in the hinterland of
1313         Neumayer station, East Antarctica. Journal of Glaciology, 56(198): 673-687.
1314     Fowler, A.C., 1992. Modelling ice sheet dynamics. Geophysical & Astrophysical Fluid
1315         Dynamics, 63(1-4): 29-65.
1316     Fretwell, P., Pritchard, H.D., Vaughan, D.G., Bamber, J.L., Barrand, N.E., Bell, R., Bianchi, C.,
1317         Bingham, R.G., Blankenship, D.D., Casassa, G., Catania, G., Callens, D., Conway, H.,
1318         Cook, A.J., Corr, H.F.J., Damaske, D., Damm, V., Ferraccioli, F., Forsberg, R., Fujita, S.,
1319         Gim, Y., Gogineni, P., Griggs, J.A., Hindmarsh, R.C.A., Holmlund, P., Holt, J.W.,
1320         Jacobel, R.W., Jenkins, A., Jokat, W., Jordan, T., King, E.C., Kohler, J., Krabill, W.,
1321         Riger-Kusk, M., Langley, K.A., Leitchenkov, G., Leuschen, C., Luyendyk, B.P.,
1322         Matsuoka, K., Mouginot, J., Nitsche, F.O., Nogi, Y., Nost, O.A., Popov, S.V., Rignot, E.,
1323         Rippin, D.M., Rivera, A., Roberts, J., Ross, N., Siegert, M.J., Smith, A.M., Steinhage, D.,
1324         Studinger, M., Sun, B., Tinto, B.K., Welch, B.C., Wilson, D., Young, D.A., Xiangbin, C.
1325         and Zirizzotti, A., 2013. Bedmap2: improved ice bed, surface and thickness datasets for
1326         Antarctica. The Cryosphere, 7(1): 375-393.
1327     Fricker, H.A., Popov, S., Allison, I. and Young, N., 2001. Distribution of marine ice beneath the
1328         Amery Ice Shelf. Geophysical Research Letters, 28(11): 2241-2244.
1329     Fricker, H.A. and Padman, L., 2006. Ice shelf grounding zone structure from ICESat laser
1330         altimetry. Geophysical Research Letters, 33(15): L15502.
1331     Fricker, H.A., Coleman, R., Padman, L., Scambos, T.A., Bohlander, J. and Brunt, K.M., 2009.
1332         Mapping the grounding zone of the Amery Ice Shelf, East Antarctica using InSAR,
1333         MODIS and ICESat. Antarctic Science, 21(5): 515-532.
1334     Fujita, S., Holmlund, P., Matsuoka, K., Enomoto, H., Fukui, K., Nakazawa, F., Sugiyama, S. and
1335         Surdyk, S., 2012. Radar diagnosis of the subglacial conditions in Dronning Maud Land,
1336         East Antarctica. The Cryosphere, 6(5): 1203-1219.
1337     Fürst, J.J., Durand, G., Gillet-Chaulet, F., Merino, N., Tavard, L., Mouginot, J., Gourmelen, N.
1338         and Gagliardini, O., 2015. Assimilation of Antarctic velocity observations provides
1339         evidence for uncharted pinning points. The Cryosphere, 9: 1427-1443.
1340     Gagliardini, O., Durand, G., Zwinger, T., Hindmarsh, R.C.A. and Le Meur, E., 2010. Coupling of
1341         ice-shelf melting and buttressing is a key process in ice-sheets dynamics. Geophys. Res.
1342         Lett., 37(14): L14501.
1343     Gillet-Chaulet, F., Hindmarsh, R.C.A., Corr, H.F.J., King, E.C. and Jenkins, A., 2011. In-situ
1344         quantification of ice rheology and direct measurement of the Raymond Effect at Summit,
1345         Greenland using a phase-sensitive radar. Geophysical Research Letters, 38: L24503.
1346     Gladish, C.V., Holland, D.M., Holland, P.R. and Price, S.F., 2012. Ice-shelf basal channels in a
1347         coupled ice/ocean model. Journal of Glaciology, 58(212): 1227-1244.
1348     Gladstone, R.M., Lee, V., Vieli, A. and Payne, A.J., 2010. Grounding line migration in an
1349         adaptive mesh ice sheet model. Journal of Geophysical Research-Earth Surface, 115:
1350         F04014.
1351     Gladstone, R.M., Lee, V., Rougier, J., Payne, A.J., Hellmer, H., Le Brocq, A., Shepherd, A.,
1352         Edwards, T.L., Gregory, J. and Cornford, S.L., 2012. Calibrated prediction of Pine Island

Glacier retreat during the 21st and 22nd centuries with a coupled flowline model. Earth and Planetary Science Letters, 333-334: 191-199.

Glasser, N.F., Kulessa, B., Luckman, A., Jansen, D., King, E.C., Sammonds, P.R., Scambos, T.A. and Jezek, K.C., 2009. Surface structure and stability of the Larsen C ice shelf, Antarctic Peninsula. Journal of Glaciology, 55(191): 400-410.

Glasser, N.F. and Gudmundsson, G.H., 2012. Longitudinal surface structures (flowstripes) on Antarctic glaciers. Cryosphere, 6(2): 383-391.

Goldberg, D., Holland, D.M. and Schoof, C., 2009. Grounding line movement and ice shelf buttressing in marine ice sheets. Journal of Geophysical Research-Earth Surface, 114: F04026.

Gomez, N., Pollard, D. and Mitrovica, J.X., 2013. A 3-D coupled ice sheet - sea level model applied to Antarctica through the last 40 ky. Earth and Planetary Science Letters, 384: 88-99.

Goodwin, A.H. and Vaughan, D.G., 1995. A topographic origin for double-ridge features in visible imagery of ice divides in Antarctica. Journal of Glaciology, 41(139): 483-489.

Goodwin, I.D. and Zweck, C., 2000. Glacio-isostasy and glacial ice load at Law Dome, Wilkes Land, East Antarctica. Quaternary Research, 53(3): 285-293.

Goodwin, I.D., Browning, S., Lorrey, A.M., Mayewski, P.A., Phipps, S.J., Bertler, N.A.N., Edwards, R.P., Cohen, T.J., van Ommen, T., Curran, M., Barr, C. and Stager, J.C., 2014. A reconstruction of extratropical Indo-Pacific sea-level pressure patterns during the Medieval Climate Anomaly. Climate Dynamics, 43(5-6): 1197-1219.

Gorodetskaya, I.V., Van Lipzig, N.P.M., Van den Broeke, M.R., Mangold, A., Boot, W. and Reijmer, C.H., 2013. Meteorological regimes and accumulation patterns at Utsteinen, Dronning Maud Land, East Antarctica: Analysis of two contrasting years. Journal of Geophysical Research-Atmospheres, 118(4): 1700-1715.

Gudmundsson, G.H., 2003. Transmission of basal variability to a glacier surface. Journal of Geophysical Research-Solid Earth, 108(B5): 2253.

Hamley, T.C., Morgan, V.I. and Thwaites, R.J., 1986. An ice-core drilling site at Law Dome summit, Wilkes Land, Antarctica. ANARE Research Notes, 37.

Haran, T.M., Bohlander, J., Scambos, T. and Fahnestock, M., 2005. MODIS mosaic of Antarctica (MOA) image map. National Snow and Ice Data Center.

Hattermann, T., Nøst, O.A., Lilly, J.M. and Smedsrud, L.H., 2012. Two years of oceanic observations below the Fimbul Ice Shelf, Antarctica. Geophys. Res. Lett., 39(12): L12605.

Hattermann, T., Smedsrud, L.H., Nost, O.A., Lilly, J.M. and Galton-Fenzi, B.K., 2014. Eddy-resolving simulations of the Fimbul Ice Shelf cavity circulation: Basal melting and exchange with open ocean. Ocean Modelling, 82: 28-44.

Hellmer, H.H. and Jacobs, S.S., 1992. Ocean interactions with the base of Amery Ice Shelf, Antarctica. Journal of Geophysical Research: Oceans, 97(C12): 20305-20317.

Hellmer, H.H., Kauker, F., Timmermann, R., Determann, J. and Rae, J., 2012. Twenty-first-century warming of a large Antarctic ice-shelf cavity by a redirected coastal current. Nature, 485(7397): 225-228.

Helm, V., Humbert, A. and Miller, H., 2014. Elevation and elevation change of Greenland and Antarctica derived from CryoSat-2. The Cryosphere, 8(4): 1539-1559.

Heroy, D.C. and Anderson, J.B., 2007. Radiocarbon constraints on Antarctic Peninsula Ice Sheet retreat following the Last Glacial Maximum (LGM). Quaternary Science Reviews, 26(25-28): 3286-3297.

Hillenbrand, C.-D., Bentley, M.J., Stolldorf, T.D., Hein, A.S., Kuhn, G., Graham, A.G.C., Fogwill, C.J., Kristoffersen, Y., Smith, J.A., Anderson, J.B., Larter, R.D., Melles, M., Hodgson, D.A., Mulvaney, R. and Sugden, D.E., 2013. Reconstruction of changes in the Weddell Sea sector of the Antarctic Ice Sheet since the Last Glacial Maximum. Quaternary Science Reviews, 100: 111-136.

Hindmarsh, R., 1996. Stochastic perturbation of divide position. Annals of Glaciology, 23: 94-104.

Hindmarsh, R.C.A., King, E.C., Mulvaney, R., Corr, H.F.J., Hiess, G. and Gillet-Chaulet, F., 2011. Flow at ice-divide triple junctions: 2. Three-dimensional views of isochrone architecture from ice-penetrating radar surveys. Journal of Geophysical Research-Earth Surface, 116: F02024.

Hofstede, C., Eisen, O., Diez, A., Jansen, D., Kristoffersen, Y., Lambrecht, A. and Mayer, C., 2013. Investigating englacial reflections with vibro- and explosive-seismic surveys at Halvfarryggen ice dome, Antarctica. Annals of Glaciology, 54(64): 189-200.

Holland, D.M. and Jenkins, A., 1999. Modeling thermodynamic ice-ocean interactions at the base of an ice shelf. Journal of Physical Oceanography, 29(8): 1787-1800.

Holland, P.R., Corr, H.F.J., Vaughan, D.G., Jenkins, A. and Skvarca, P., 2009. Marine ice in Larsen Ice Shelf. Geophysical Research Letters, 36: L11604.

Horgan, H.J. and Anandakrishnan, S., 2006. Static grounding lines and dynamic ice streams: Evidence from the Siple Coast, West Antarctica. Geophysical Research Letters, 33(18): L18502.

Hughes, T., 1973. Is the west Antarctic Ice Sheet disintegrating? Journal of Geophysical Research, 78(33): 7884-7910.

Hulbe, C. and Fahnestock, M., 2007. Century-scale discharge stagnation and reactivation of the Ross ice streams, West Antarctica. Journal of Geophysical Research-Earth Surface, 112: F03S27.

Hulbe, C.L., LeDoux, C. and Cruikshank, K., 2010. Propagation of long fractures in the Ronne Ice Shelf, Antarctica, investigated using a numerical model of fracture propagation. Journal of Glaciology, 56(197): 459-472.

Humbert, A. and Steinhage, D., 2011. The evolution of the western rift area of the Fimbul Ice Shelf, Antarctica. Cryosphere, 5(4): 931-944.

Hvidberg, C.S., 1996. Steady-state thermomechanical modelling of ice flow near the center of large ice sheets with the finite-element technique. Annals of Glaciology, 23: 116-123.

Jacobs, S.S. and Comiso, J.C., 1989. Sea ice and oceanic processes on the Ross Sea continental shelf. Journal of Geophysical Research: Oceans, 94(C12): 18195-18211.

Jacobs, S.S., Helmer, H.H., Doake, C.S.M., Jenkins, A. and Frolich, R.M., 1992. Melting of ice shelves and the mass balance of Antarctica. Journal of Glaciology, 38(130): 375-387.

Jacobs, S.S., Jenkins, A., Giulivi, C.F. and Dutrieux, P., 2011. Stronger ocean circulation and increased melting under Pine Island Glacier ice shelf. Nature Geoscience, 4(8): 519-523.

Jacobson, H.P. and Waddington, E.D., 2004. Recumbent folding in ice sheets: a core-referential study. Journal of Glaciology, 50(168): 3-16.

Jansen, D., Luckman, A., Kulessa, B., Holland, P.R. and King, E.C., 2013. Marine ice formation in a suture zone on the Larsen C Ice Shelf and its influence on ice shelf dynamics. Journal of Geophysical Research: Earth Surface, 118(3): 1628-1640.

Jenkins, A., Dutrieux, P., Jacobs, S.S., McPhail, S.D., Perrett, J.R., Webb, A.T. and White, D., 2010a. Observations beneath Pine Island Glacier in West Antarctica and implications for its retreat. Nature Geoscience, 3(7): 468-472.

Jenkins, A., Nicholls, K.W. and Corr, H.F.J., 2010b. Observation and Parameterization of Ablation at the Base of Ronne Ice Shelf, Antarctica. Journal of Physical Oceanography, 40(10): 2298-2312.

Jezek, K.C., 1984. A modified theory of bottom crevasses used as a means for measuring the buttressing effect of ice shelves on inland ice sheets. Journal of Geophysical Research: Solid Earth, 89(B3): 1925-1931.

Jezek, K.C. and Team, R.P., 2002. RAMP AMM-1 SAR Image Mosaic of Antarctica. Version 2.

Joughin, I. and Padman, L., 2003. Melting and freezing beneath Filchner-Ronne Ice Shelf, Antarctica. Geophysical Research Letters, 30(9): 1477.

Joughin, I., Smith, B.E. and Medley, B., 2014. Marine Ice Sheet Collapse Potentially Underway for the Thwaites Glacier Basin, West Antarctica. Science, 344(6185): 735-738.

Khazendar, A., Tison, J.L., Stenni, B., Dini, M. and Bondesan, A., 2001. Significant marine-ice accumulation in the ablation zone beneath an Antarctic ice shelf. Journal of Glaciology, 47(158): 359-368.

Kim, K.T., Jezek, K.C. and Sohn, H.G., 2001. Ice shelf advance and retreat rates along the coast of Queen Maud Land, Antarctica. Journal of Geophysical Research-Oceans, 106(C4): 7097-7106.

King, J.C., Anderson, P.S., Vaughan, D.G., Mann, G.W., Mobbs, S.D. and Vosper, S.B., 2004. Wind-borne redistribution of snow across an Antarctic ice rise. Journal of Geophysical Research-Atmospheres, 109: D11104.

Kingslake, J., Hindmarsh, R.C.A., Aðalgeirsdóttir, G., Conway, H., Corr, H.F.J., Gillet-Chaulet, F., Martín, C., King, E.C., Mulvaney, R. and Pritchard, H.D., 2014. Full-depth englacial vertical ice sheet velocities measured using phase-sensitive radar. Journal of Geophysical Research: Earth Surface, 119: JF003275.

Kulessa, B., Jansen, D., Luckman, A.J., King, E.C. and Sammonds, P.R., 2014. Marine ice regulates the future stability of a large Antarctic ice shelf. Nat Commun, 5: 3707.

Lange, M.A. and MacAyeal, D.R., 1986. Numerical models of the Filchner-Ronne ice shelf - An assessment of reinterpreted ice thickness distributions. Journal of Geophysical Research-Solid Earth and Planets, 91(B10): 457-462.

Lenaerts, J.T.M. and van den Broeke, M.R., 2012. Modeling drifting snow in Antarctica with a regional climate model: 2. Results. Journal of Geophysical Research-Atmospheres, 117: D05109.

Lenaerts, J.T.M., van den Broeke, M.R., van de Berg, W.J., van Meijgaard, E. and Kuipers Munneke, P., 2012. A new, high-resolution surface mass balance map of Antarctica (1979-2010) based on regional atmospheric climate modeling. Geophys. Res. Lett., 39(4): L04501.

Lenaerts, J.T.M., Brown, J., Van Den Broeke, M.R., Matsuoka, K., Drews, R., Callens, D., Philippe, M., Gorodetskaya, I.V., Van Meijgaard, E., Reijmer, C.H., Pattyn, F. and Van Lipzig, N.P.M., 2014. High variability of climate and surface mass balance induced by Antarctic ice rises. Journal of Glaciology, 60(224): 1101-1110.

Limbert, D.W., 1964. The absolute and relative movement, and regime of the Brunt Ice Shelf near Helley Bay. British Antarctic Survey Bulletin, 3: 1-11.

MacAyeal, D.R., Bindschadler, R.A., Shabtaie, S., Stephenson, S. and Bentley, C.R., 1987. Force, mass, and energy budgets of the Crary Ice Rise complex, Antarctica. Journal of Glaciology, 33(114): 218-230.

MacGregor, J.A., Winebrenner, D.P., Conway, H., Matsuoka, K., Mayewski, P.A. and Clow, G.D., 2007. Modeling englacial radar attenuation at Siple Dome, West Antarctica, using

ice chemistry and temperature data. Journal of Geophysical Research-Earth Surface, 112(F3): doi:10.1029/2006JF000717.

Mackintosh, A.N., Verleyen, E., O'Brien, P.E., White, D.A., Jones, R.S., McKay, R., Dunbar, R., Gore, D.B., Fink, D., Post, A.L., Miura, H., Leventer, A., Goodwin, I., Hodgson, D.A., Lilly, K., Crosta, X., Golledge, N.R., Wagner, B., Berg, S., van Ommen, T., Zwartz, D., Roberts, S.J., Vyverman, W. and Masse, G., 2013. Retreat history of the East Antarctic Ice Sheet since the Last Glacial Maximum. Quaternary Science Reviews, 100: 10-30.

Makinson, K. and Nicholls, K.W., 1999. Modeling tidal currents beneath Filchner-Ronne Ice Shelf and on the adjacent continental shelf: their effect on mixing and transport. Journal of Geophysical Research-Oceans, 104(C6): 13449-13465.

Makinson, K., Holland, P.R., Jenkins, A., Nicholls, K.W. and Holland, D.M., 2010. Influence of tides on melting and freezing beneath Filchner-Ronne Ice Shelf, Antarctica. Geophysical Research Letters, 38.

Martin, C., Hindmarsh, R.C.A. and Navarro, F.J., 2006. Dating ice flow change near the flow divide at Roosevelt Island, Antarctica, by using a thermomechanical model to predict radar stratigraphy. Journal of Geophysical Research-Earth Surface, 111: F01011.

Martin, C., Gudmundsson, G.H., Pritchard, H.D. and Gagliardini, O., 2009a. On the effects of anisotropic rheology on ice flow, internal structure, and the age-depth relationship at ice divides. Journal of Geophysical Research-Earth Surface, 114: F04001.

Martin, C., Hindmarsh, R.C.A. and Navarro, F.J., 2009b. On the effects of divide migration, along-ridge flow, and basal sliding on isochrones near an ice divide. Journal of Geophysical Research-Oceans, 114: F02006.

Martin, C. and Gudmundsson, G.H., 2012. Effects of nonlinear rheology, temperature and anisotropy on the relationship between age and depth at ice divides. Cryosphere, 6(5): 1221-1229.

Martin, C., Gudmundsson, G.H. and King, E.C., 2014. Modelling of Kealey Ice Rise, Antarctica, reveals stable ice-flow conditions in East Ellsworth Land over millennia. Journal of Glaciology, 60(219): 139-146.

Martin, P.J., 1976. Ridges on Antarctic ice rises. Journal of Glaciology, 17(75): 141-144.

Martin, P.J. and Sanderson, T.J.O., 1980. Morphology and dynamics of ice rises. Journal of Glaciology, 25(91): 33-45.

Massom, R.A., Giles, A.B., Fricker, H.A., Warner, R.C., Legresy, B., Hyland, G., Young, N. and Fraser, A.D., 2010. Examining the interaction between multi-year landfast sea ice and the Mertz Glacier Tongue, East Antarctica: Another factor in ice sheet stability? Journal of Geophysical Research-Oceans, 115: C12027.

Matsuoka, K., Pattyn, F., Callens, D. and Conway, H., 2012. Radar characterization of the basal interface across the grounding zone of an ice-rise promontory in East Antarctica. Annals of Glaciology, 53(60): 29-36.

Miles, B.W.J., Stokes, C.R., Vieli, A. and Cox, N.J., 2013. Rapid, climate-driven changes in outlet glaciers on the Pacific coast of East Antarctica. Nature, 500(7464): 563-566.

Morgan, V.I., Wookey, C.W., Li, J., vanOmmen, T.D., Skinner, W. and Fitzpatrick, M.F., 1997. Site information and initial results from deep ice drilling on Law dome, Antarctica. Journal of Glaciology, 43(143): 3-10.

Mulvaney, R., Alemany, O. and Possenti, P., 2007. The Berkner Island (Antarctica) ice-core drilling project. Annals of Glaciology, 47(1): 115-124.

Mulvaney, R., Triest, J. and Alemany, O., 2014. The James Ross Island and the Fletcher Promontory ice-core drilling projects. Annals of Glaciology, 55(68): 179-188.

Naik, S.S., Thamban, M., Laluraj, C.M., Redkar, B.L. and Chaturvedi, A., 2010. A century of climate variability in central Dronning Maud Land, East Antarctica, and its relation to Southern Annular Mode and El Nino-Southern Oscillation. Journal of Geophysical Research-Atmospheres, 115(D16): D16102.

Nereson, N.A., Hindmarsh, R.C.A. and Raymond, C.F., 1998a. Sensitivity of the divide position at Siple Dome, West Antarctica, to boundary forcing. Annals of Glaciology, 27: 207-214.

Nereson, N.A., Raymond, C.F., Waddington, E.D. and Jacobel, R.W., 1998b. Migration of the Siple Dome ice divide, West Antarctica. Journal of Glaciology, 44(148): 643-652.

Nereson, N.A., Raymond, C.F., Jacobel, R.W. and Waddington, E.D., 2000. The accumulation pattern across Siple Dome, West Antarctica, inferred from radar-detected internal layers. Journal of Glaciology, 46(152): 75-87.

Nereson, N.A. and Raymond, C.F., 2001. The elevation history of ice streams and the spatial accumulation pattern along the Siple Coast of West Antarctica inferred from ground-based radar data from three inter-ice-stream ridges. Journal of Glaciology, 47(157): 303-313.

Nereson, N.A. and Waddington, E.D., 2002. Isochrones and isotherms beneath migrating ice divides. Journal of Glaciology, 48(160): 95-108.

Neumann, T.A., Conway, H., Price, P.B., Waddington, E.D., Catania, G. and Morse, D.L., 2008. Holocene accumulation and ice-sheet dynamics in central West Antarctica. Journal of Geophysical Research, 113(F02018): doi:10.1029/2007JF000764.

Nicholls, K.W., Osterhus, S., Makinson, K. and Johnson, M.R., 2001. Oceanographic conditions south of Berkner Island, beneath Filchner-Ronne Ice Shelf, Antarctica. Journal of Geophysical Research-Oceans, 106(C6): 11481-11492.

Nicholls, K.W., Osterhus, S., Makinson, K., Gammelsrod, T. and Fahrbach, E., 2009. Ice-ocean processes over the continental shelf of the Southern Weddell Sea, Antarctica: a review. Reviews of Geophysics, 47: Rg3003.

Nost, O.A., Biuw, M., Tverberg, V., Lydersen, C., Hattermann, T., Zhou, Q., Smedsrud, L.H. and Kovacs, K.M., 2011. Eddy overturning of the Antarctic Slope Front controls glacial melting in the Eastern Weddell Sea. Journal of Geophysical Research-Oceans, 116: C11014.

Padman, L., Erofeeva, S. and Joughin, I., 2003. Tides of the Ross Sea and Ross Ice Shelf cavity. Antarctic Science, 15(1): 31-40.

Parrenin, F. and Hindmarsh, R., 2007. Influence of a non-uniform velocity field on isochrone geometry along a steady flowline of an ice sheet. Journal of Glaciology, 53(183): 612-622.

Pattyn, F., 2010. Antarctic subglacial conditions inferred from a hybrid ice sheet/ice stream model. Earth and Planetary Science Letters, 295(3-4): 451-461.

Pattyn, F., Matsuoka, K., Callens, D., Conway, H., Depoorter, M., Docquier, D., Hubbard, B., Samyn, D. and Tison, J.L., 2012a. Melting and refreezing beneath Roi Baudouin Ice Shelf (East Antarctica) inferred from radar, GPS, and ice core data. J. Geophys. Res., 117(F4): F04008.

Pattyn, F., Schoof, C., Perichon, L., Hindmarsh, R.C.A., Bueler, E., de Fleurian, B., Durand, G., Gagliardini, O., Gladstone, R., Goldberg, D., Gudmundsson, G.H., Huybrechts, P., Lee, V., Nick, F.M., Payne, A.J., Pollard, D., Rybak, O., Saito, F. and Vieli, A., 2012b. Results of the Marine Ice Sheet Model Intercomparison Project, MISMIP. The Cryosphere, 6(3): 573-588.

1587 Pettit, E.C., Jacobson, H.P. and Waddington, E.D., 2003. Effects of basal sliding on isochrones
1588         and flow near an ice divide. Annals of Glaciology, 37: 370-376.
1589 Pettit, E.C., Thorsteinsson, T., Jacobson, H.P. and Waddington, E.D., 2007. The role of crystal
1590         fabric in flow near an ice divide. Journal of Glaciology, 53(181): 277-288.
1591 Pettit, E.C., Waddington, E.D., Harrison, W.D., Thorsteinsson, T., Elsberg, D., Morack, J. and
1592         Zumberge, M.A., 2011. The crossover stress, anisotropy and the ice flow law at Siple
1593         Dome, West Antarctica. Journal of Glaciology, 57(201): 39-52.
1594 Petty, A.A., Feltham, D.L. and Holland, P.R., 2013. Impact of Atmospheric Forcing on Antarctic
1595         Continental Shelf Water Masses. Journal of Physical Oceanography, 43(5): 920-940.
1596 Pollard, D. and DeConto, R.M., 2009. Modelling West Antarctic ice sheet growth and collapse
1597         through the past five million years. Nature, 458(7236): 329-332.
1598 Pollard, D. and DeConto, R.M., 2012. Description of a hybrid ice sheet-shelf model, and
1599         application to Antarctica. Geoscientific Model Development, 5(5): 1273-1295.
1600 Price, S.F., Conway, H. and Waddington, E.D., 2007. Evidence for late pleistocene thinning of
1601         Siple Dome, West Antarctica. Journal of Geophysical Research-Earth Surface, 112(F3):
1602         F03021.
1603 Pritchard, H.D., Ligtenberg, S.R.M., Fricker, H.A., Vaughan, D.G., van den Broeke, M.R. and
1604         Padman, L., 2012. Antarctic ice-sheet loss driven by basal melting of ice shelves. Nature,
1605         484(7395): 502-505.
1606 Raymond, C.F., 1983. Deformation in the vicinity of ice divides. Journal of Glaciology, 29(103):
1607         357-373.
1608 Raymond, C.F., Nereson, N.A. and Conway, H., 1995. Geometry and stratigraphy of Siple Dome,
1609         Antarctica. Antarctic Journal of the United States, 30(5): 91-93.
1610 Rex, R.W., Margolis, S.V. and Murray, B., 1970. Possible interglacial dune sands from 300
1611         meters water depth in Weddell-Sea, Antarctica. Geological Society of America Bulletin,
1612         81(11): 3465-3472.
1613 Rignot, E., 2002. Ice-shelf changes in Pine Island Bay, Antarctica, 1947-2000. Journal of
1614         Glaciology, 48(161): 247-256.
1615 Rignot, E., 2008. Changes in West Antarctic ice stream dynamics observed with ALOS PALSAR
1616         data. Geophysical Research Letters, 35(12): L12505.
1617 Rignot, E., Mouginot, J. and Scheuchl, B., 2011. Ice Flow of the Antarctic Ice Sheet. Science,
1618         333(6048): 1427-1430.
1619 Rignot, E., Jacobs, S., Mouginot, J. and Scheuchl, B., 2013. Ice Shelf Melting Around Antarctica.
1620         Science, 341(6143): 266-270.
1621 Rignot, E., Mouginot, J., Morlighem, M., Seroussi, H. and Scheuchl, B., 2014. Widespread, rapid
1622         grounding line retreat of Pine Island, Thwaites, Smith, and Kohler glaciers, West
1623         Antarctica, from 1992 to 2011. Geophysical Research Letters, 41(10): 3502-3509.
1624 Roberts, J.L., Moy, A.D., van Ommen, T.D., Curran, M.A.J., Worby, A.P., Goodwin, I.D. and
1625         Inoue, M., 2013. Borehole temperatures reveal a changed energy budget at Mill Island,
1626         East Antarctica, over recent decades. Cryosphere, 7(1): 263-273.
1627 Robin, G.D., 1953. Measurements of ice thickness in Dronning Maud Land, Antarctica. Nature,
1628         171(4341): 55-58.
1629 Scambos, T.A., Haran, T.M., Fahnestock, M.A., Painter, T.H. and Bohlander, J., 2007. MODIS-
1630         based Mosaic of Antarctica (MOA) data sets: Continent-wide surface morphology and
1631         snow grain size. Remote Sensing of Environment, 111(2-3): 242-257.
1632 Schmeltz, M., Rignot, E. and Macayeal, D.R., 2001. Ephemeral grounding as a signal of ice-shelf
1633         change. Journal of Glaciology, 47(156): 71-77.

Schoof, C., 2007. Ice sheet grounding line dynamics: Steady states, stability, and hysteresis. Journal of Geophysical Research-Earth Surface, 112(F3): F03S28.

Schoof, C. and Hindmarsh, R.C.A., 2010. Thin-Film Flows with Wall Slip: An Asymptotic Analysis of Higher Order Glacier Flow Models. Quarterly Journal of Mechanics and Applied Mathematics, 63(1): 73-114.

Scientific Committee on Antarctic Research, 2012, Antarctic Digital Database version 6.0.

Sergienko, O.V., 2013. Basal channels on ice shelves. Journal of Geophysical Research: Earth Surface, 118: 1342-1355.

Shipp, S., Anderson, J. and Domack, E., 1999. Late Pleistocene-Holocene retreat of the West Antarctic Ice-Sheet system in the Ross Sea: Part 1 - Geophysical results. Geological Society of America Bulletin, 111(10): 1486-1516.

Siegert, M., Ross, N., Corr, H., Kingslake, J. and Hindmarsh, R., 2013. Late Holocene ice-flow reconfiguration in the Weddell Sea sector of West Antarctica. Quaternary Science Reviews, 78(0): 98-107.

Sinclair, K.E., Bertler, N.A.N., Bowen, M.M. and Arrigo, K.R., 2014. Twentieth century sea-ice trends in the Ross Sea from a high-resolution, coastal ice-core record. Geophysical Research Letters, 41(10): 3510-3516.

Smith, A.M., 1986. Ice rumples on Ronne Ice Shelf, Antarctica. British Antarctic Survey Bulletin, 72: 47-52.

Smith, A.M., 1991. The use of tiltmeters to study the dynamics of Antarctic ice-shelf grounding lines. Journal of Glaciology, 37(125): 51-58.

Stewart, A.L. and Thompson, A.F., 2015. Eddy-mediated transport of warm Circumpolar Deep Water across the Antarctic Shelf Break. Geophysical Research Letters, 42(2): 432-440.

Stone, J.O., Balco, G.A., Sugden, D.E., Caffee, M.W., Sass, L.C., Cowdery, S.G. and Siddoway, C., 2003. Holocene deglaciation of Marie Byrd Land, West Antarctica. Science, 299(5603): 99-102.

Swithinbank, C., 1977. Glaciological Research in the Antarctic Peninsula. Philosophical Transactions of the Royal Society of London Series B, 279: 161-183.

Tamura, T., Ohshima, K.I. and Nihashi, S., 2008. Mapping of sea ice production for Antarctic coastal polynyas. Geophysical Research Letters, 35(7): L07606.

Taylor, K.C., Alley, R.B., Meese, D.A., Spencer, M.K., Brook, E.J., Dunbar, N.W., Finkel, R.C., Gow, A.J., Kurbatov, A.V., Lamorey, G.W., Mayewski, P.A., Meyerson, E.A., Nishiizumi, K. and Zielinski, G.A., 2004. Dating the Siple Dome (Antarctica) ice core by manual and computer interpretation of annual layering. Journal of Glaciology, 50(170): 453-461.

Thoma, M., Jenkins, A., Holland, D. and Jacobs, S., 2008. Modelling Circumpolar Deep Water intrusions on the Amundsen Sea continental shelf, Antarctica. Geophysical Research Letters, 35: L18602.

Thomas, E.R., Marshall, G.J. and McConnell, J.R., 2008. A doubling in snow accumulation in the western Antarctic Peninsula since 1850. Geophysical Research Letters, 35: L01706.

Thomas, R.H., 1971. Flow law for Antarctic ice shelves. Nature-Physical Science, 232(30): 85-87.

Thomas, R.H., 1973a. The creep of ice shelves: theory. Journal of Glaciology, 12(64): 45-53.

Thomas, R.H., 1973b. The creep of ice shelves: interpretation of observed behavior. Journal of Glaciology, 12(64): 55-70.

Thomas, R.H., 1979. Ice shelves: a review. Journal of Glaciology, 24(90): 167-177.

1680 Thomas, R.H. and MacAyeal, D.R., 1982. Derived characteristics of the Ross Ice Shelf,
1681    Antarctica. Journal of Glaciology, 28(100): 397-412.
1682 Tinto, K.J. and Bell, R.E., 2011. Progressive unpinning of Thwaites Glacier from newly
1683    identified offshore ridge: Constraints from aerogravity. Geophysical Research Letters, 38:
1684    L20503.
1685 Van de Berg, W.J., van den Broeke, M.R., Reijmer, C.H. and van Meijgaard, E., 2006.
1686    Reassessment of the Antarctic surface mass balance using calibrated output of a regional
1687    atmospheric climate model. Journal of Geophysical Research-Atmospheres, 111(D11):
1688    D11104.
1689 van den Broeke, M., van de Berg, W.J. and van Meijgaard, E., 2006. Snowfall in coastal West
1690    Antarctica much greater than previously assumed. Geophysical Research Letters, 33:
1691    L02505.
1692 Van Lipzig, N.P.M., Turner, J., Colwell, S.R. and Van Den Broeke, M.R., 2004. The near-surface
1693    wind field over the Antarctic continent. International Journal of Climatology, 24(15):
1694    1973-1982.
1695 Van Ommen, T.D., Morgan, V. and Curran, M.A.J., 2004. Deglacial and Holocene changes in
1696    accumulation at Law Dome, East Antarctica. Annals of Glaciology, 39: 359-365.
1697 Vaughan, D.G., Corr, H.F.J., Doake, C.S.M. and Waddington, E.D., 1999. Distortion of
1698    isochronous layers in ice revealed by ground-penetrating radar. Nature, 398(6725): 323-
1699    326.
1700 Vaughan, D.G., Marshall, G.J., Connolley, W.M., Parkinson, C., Mulvaney, R., Hodgson, D.A.,
1701    King, J.C., Pudsey, C.J. and Turner, J., 2003. Recent rapid regional climate warming on
1702    the Antarctic Peninsula. Climatic Change, 60(3): 243-274.
1703 Vaughan, D.G., Anderson, P.S., King, J.C., Mann, G.W., Mobbs, S.D. and Ladkin, R.S., 2004.
1704    Imaging of firn isochrones across an Antarctic ice rise and implications for patterns of
1705    snow accumulation rate. Journal of Glaciology, 50(170): 413-418.
1706 Waddington, E.D., Conway, H., Steig, E.J., Alley, R.B., Brook, E.J., Taylor, K.C. and White,
1707    J.W.C., 2005. Decoding the dipstick: Thickness of Siple Dome, West Antarctica, at the
1708    Last Glacial Maximum. Geology, 33(4): 281-284.
1709 Waddington, E.D., Neumann, T.A., Koutnik, M.R., Marshall, H.P. and Morse, D.L., 2007.
1710    Inference of accumulation-rate patterns from deep layers in glaciers and ice sheets.
1711    Journal of Glaciology, 53(183): 694-712.
1712 Wang, W.L., Warner, R.C. and Budd, W.F., 2002. Ice-flow properties at Dome Summit South,
1713    Law Dome, East Antarctica. Annals of Glaciology, 35: 567-573.
1714 Weber, M.E., Clark, P.U., Kuhn, G., Timmermann, A., Sprenk, D., Gladstone, R., Zhang, X.,
1715    Lohmann, G., Menviel, L., Chikamoto, M.O., Friedrich, T. and Ohlwein, C., 2014.
1716    Millennial-scale variability in Antarctic ice-sheet discharge during the last deglaciation.
1717    Nature, 510(7503): 134-138.
1718 Weertman, J., 1974. Stability of the junction of an ice sheet and an iec shelf. Journal of
1719    Glaciology, 13(67): 3-11.
1720 Whillans, I.M., 1973. State of equilibrium of west Antarctic inland ice sheet. Science, 182(4111):
1721    476-479.
1722 Whitehouse, P.L., Bentley, M.J., Milne, G.A., King, M.A. and Thomas, I.D., 2012. A new glacial
1723    isostatic adjustment model for Antarctica: calibrated and tested using observations of
1724    relative sea-level change and present-day uplift rates. Geophysical Journal International,
1725    190(3): 1464-1482.

1726　Wilson, D.S. and Luyendyk, B.P., 2006. Bedrock platforms within the Ross Embayment, West
1727　　　Antarctica: Hypotheses for ice sheet history, wave erosion, Cenozoic extension, and
1728　　　thermal subsidence. Geochem. Geophys. Geosyst., 7(12): Q12011.
1729　Zhou, Q., Hattermann, T., Nøst, O.A., Biuw, M., Kovacs, K.M. and Lydersen, C., 2014. Wind-
1730　　　driven spreading of fresh surface water beneath ice shelves in the Eastern Weddell Sea.
1731　　　Journal of Geophysical Research: Oceans, 119(6): 3818-3833.
1732
1733

1734